Challenges in Simulating Ozone Depletion Events in the Arctic Boundary Layer: A Case Study Using ECHAM/MESSy for Spring 2019/20

Stefanie Falk¹, Luca Reißig¹, Bianca Zilker², Andreas Richter², and Björn-Martin Sinnhuber¹

Correspondence: Stefanie Falk (stefanie.falk@kit.edu)

Abstract. Ozone depletion events (ODEs) and bromine explosions (BEs) occur regularly in the springtime polar boundary layer. ODEs alter the oxidation capacity of the polar boundary layer and promote formation of toxic mercury. We investigated Arctic ODEs and BEs in 2019/20 using the chemistry-climate model ECHAM/MESSy v2.55.2, nudged with ERA5 reanalysis data. Model results were evaluated against surface ozone measurements, satellite-derived tropospheric BrO vertical column densities (VCDs), and in situ data from the MOSAiC expedition. The model underestimated boundary layer (BL) height during shallow BL conditions, coinciding with a warm surface temperature bias $(2-10\,\mathrm{K})$, particularly below $-10\,^\circ\mathrm{C}$, likely inherited from ERA5. An updated model configuration, incorporating more realistic multi-year sea ice and relaxed bromine release thresholds, improved agreement with coastal ozone observations (Eureka, Utqiagvik) but still failed to reproduce strong ODEs observed during MOSAiC. Consequently, modeled surface BrO mixing ratios were overestimated, while BrO VCDs were underestimated, suggesting that simply increasing Br₂ emissions does not resolve discrepancies. A weaker colocation between modeled BrO VCDs and ODEs aligns with prior airborne studies and may reflect tropospheric chemical and transport processes rather than stratospheric contributions. Despite decreasing Arctic sea ice extent and increasing BrO VCDs, long-term records from Alert, Utqiagvik, and Zeppelin show a decline in strong ODE frequency since 2008. This suggests that bromine emissions from first-year sea ice alone may not fully account for observed ODE variability, and that additional climate-sensitive mechanisms may modulate Arctic ozone chemistry. Long-term model integrations are recommended to better understand these trends.

1 Introduction

The Arctic is subject to rapid changes due to the warming climate (AMAP, 2012; Rantanen et al., 2022). The impact of this change is reflected by the decrease of sea ice extent and thickness over the past decades (Stroeve and Notz, 2018; Lindsay and Schweiger, 2015) which caused a decline in multi-year sea ice and a stronger seasonality of the ice cover (Haine and Martin, 2017). Sea ice extent and thickness are projected to further decrease in all future projections (Notz and SIMIP Community, 2020) which may open new routes for cargo ships towards the end of the 21st century with an associated increase in Arctic

¹Institute of Meteorology and Climate Research, Atmospheric Trace Gases and Remote Sensing, Karlsruhe Institute of Technology, Karlsruhe, Germany

²Institute of Environmental Physics, University of Bremen, Bremen, Germany

air pollution (Yumashev et al., 2017). The composition of the Arctic troposphere in winter and spring is strongly affected by long-range transport from mid-latitudes, while the polar dome prevents this transport in summer (Bozem et al., 2019). Primary pollutants include NO_x and CO, which are precursor substances for the formation of tropospheric ozone (O_3) after polar sunrise. Annual mean ozone volume mixing ratios (VMRs) at the surface are relatively low in the Arctic ($\chi_{O_3} \leq 30 \,\mathrm{ppbv}$) compared to the mid-latitudes of the northern hemisphere and show a distinct seasonal cycle with a polar winter maximum (October–February) and a polar summer minimum (March/April–August/September) (Helmig et al., 2007; Whaley et al., 2023).

Tropospheric ozone VMR has been observed to drop below the detection limit on sites near the Arctic Ocean in springtime (March–May) for decades. These periods of $\chi_{\rm O_3} \leq 5\,\mathrm{ppbv}$, sometimes extending for several days, were first recognized by Bottenheim et al. (1986) in Alert (Canada), who coined the term Ozone Depletion Events (ODEs). Later, satellite observations revealed coincident plumes of enhanced bromine monoxide (BrO) vertical column densities (VCDs) extending over synoptic scales in both Arctic and Antarctic regions (Richter et al., 1998; Wagner and Platt, 1998; Richter et al., 2002). This was evidence that bromine (Br) chemistry leads to the destruction of ozone during ODEs (Barrie et al., 1988; McConnell et al., 1992; Platt and Hönninger, 2003). The associated chemical mechanism also alters the oxidation capacity of the polar boundary layer and affects formation of toxic, oxidized mercury (Brooks et al., 2006; Wang et al., 2019c) that accumulates up the food chain and causes serious health issues.

30

With polar sunrise, molecular bromine (Br_2) is photo-dissociated (Eq. (R1)) and subsequently destroys O_3 forming BrO 40 (Eq. (R2)):

$$Br_2 + h\nu \rightarrow 2Br,$$
 (R1)

$$Br + O_3 \rightarrow BrO + O_2$$
. (R2)

The resulting BrO can then self-react to form both Br and Br₂ (Eq. (R3)) or react with hydroperoxyl (HO₂) to form hypobromous acid (HOBr) (Eq. (R4)), which photo-dissociates to Br (Eq. (R5)) starting the cycle again:

45 BrO + BrO
$$\rightarrow$$

$$\begin{cases} 2Br + O_2 \\ Br_2 + O_2 \end{cases}$$
, (R3)

$$BrO + HO_2 \rightarrow HOBr + O_2,$$
 (R4)

$$HOBr + h\nu \rightarrow OH + Br.$$
 (R5)

These reactions terminate with the formation of reservoir species such as hydrogen bromide (HBr) that are not efficient at forming reactive bromine. The main source of inorganic bromine in the polar regions is bromide (Br $^-$) from sea salt (Koop et al., 2000). It is continually emitted from the open ocean or open leads in the sea ice. Sea salt aerosols release Br $_2$ into the gas-phase (Yang et al., 2005). A minor contribution comes from organic bromine (for example CHBr $_3$, CH $_2$ Br $_2$, CH $_3$ Br) emitted from ocean and sea ice (Stemmler et al., 2015; Abrahamsson et al., 2018). Recycling of inorganic bromine is necessary to sustain ODEs (Abbatt et al., 2012). This can involve heterogeneous and multiphase reactions of, for example, HOBr or bromine nitrate (BrNO $_3$) on salty ice surfaces or in salty solutions (Sander et al., 2006):

55
$$HOBr + \begin{cases} Br_{aq}^{-} & \xrightarrow{H^{+}} \begin{cases} Br_{2} \\ BrCl \end{cases} + H_{2}O,$$
 (R6)

$$BrNO_3 + \begin{cases} Br_{aq}^- \\ Cl_{aq}^- \end{cases} \rightarrow \begin{cases} Br_2 \\ BrCl \end{cases} + NO_3^-.$$
(R7)

Interhalogen reactions are able to turn BrCl into Br₂:

$$BrCl + Br^- \rightleftharpoons Br_2Cl^- \rightleftharpoons Br_2 + Cl^-.$$
 (R8)

For each brominated trace gas in Eqs. (R6)–(R7) getting in contact with an icy surface of high salinity, twice the number of bromine atoms is released. This exponential increase is called bromine explosion (BE).

This mechanism is well understood through lab experiments (Fickert et al., 1999; Adams et al., 2002) and physicochemical aspects of bromide oxidation on salty ice surfaces including the role of acidity and temperature have been studied in detail (Wren et al., 2010; Oldridge and Abbatt, 2011). Box modeling (Sander et al., 2006) and one-dimensional model studies that also includes deeper snow layers (Toyota et al., 2014) have shown that the picture is far from complete and that liquid-phase reactions also play an important role in deeper snow layers. Accurate predictions on a larger scale still pose a challenge for Chemistry Transport (CTMs) and Chemistry-Climate Models (CCMs) in their default setup (Whaley et al., 2023).

Observational evidence indicates that BEs occur in two distinct synoptic situations: stable boundary layer (BL) with little mixing, and turbulent mixing during blizzards (Hausmann and Platt, 1994; Jones et al., 2009; Zhao et al., 2016). This is reflected by two distinct mechanisms for bromine release implemented into models: (1) surface bulk snow and ice (Toyota et al., 2011) and (2) blowing snow emissions (Yang et al., 2008, 2010). Marelle et al. (2021) showed that bromine emissions from bulk snow and ice dominate over those from blowing snow in triggering ODEs while blowing snow is an important additional source of sea salt aerosols.

Latest satellite observations of BrO VCDs with a high spatial resolution (Seo et al., 2019, 2020) indicate that snow-covered first-year sea ice in combination with open leads and sea ice cracks may act as the primary source of bromide during BEs which is in contrast to earlier findings that showed no coincidence between these sea ice features and the intensity of ozone depletion (Ridley et al., 2003).

This work aims at a better understanding and characterization of the bromine release from sea ice and surface snow and the subsequent BEs and ODEs in the global CCM ECHAM/MESSy Atmospheric Chemistry (EMAC) model (Jöckel et al., 2005, 2016). To assess the model's performance in the central Arctic, we utilize observational data from the 2019/20 season, corresponding to the Multidisciplinary drifting Observatory for the Study of Arctic Climate (MOSAiC) expedition. In Sect. 2, we describe the EMAC model and present the observational data sets used for model evaluation. The observational data consist of O₃ VMRs at Arctic ozone monitoring sites and satellite BrO VCD at high resolution from the TROPOMI instrument onboard the Copernicus Sentinel-5P satellite. Subsequently, we identify the best model setup based on spring 2019 conditions (Sect. 3). Results using this best setup are compared to observational data for spring 2020 especially accounting for measurements taken during the MOSAiC expedition. Implications on pan-Arctic and site-specific climatological ozone depletion trends as well as BrO VCDs are presented in Sect. 4. Finally, we discuss (Sect. 5) and summarize our results giving a brief outlook in Sect. 6.

2 Methods and data

90

95

100

105

2.1 Model description and setup

We use the Modular Earth Submodel System (MESSy) v2.55.2 in combination with basemodel ECHAM5.2 (ECHAM/MESSy) referred to as EMAC. MESSy is a software framework that combines Earth system components, such as atmosphere, land, ocean, and subsystems of these, in a modular way (Jöckel et al., 2005, 2016). This modularity enables the deployment of different basemodels with an identical numerical implementation of geophysical and -chemical processes and parameterization.

We base the EMAC model setup on REF-C1SD of the Chemistry Climate Model Initiative (CCMI) 2 (Orbe et al., 2020). We use specified dynamics (SD) for the historical period 2019/20, with nudged surface pressure (logarithmic) and nudged temperature, divergence, and vorticity fields from above the boundary layer (model level 8) up to a pressure level of 1hPa. Sea Surface Temperatures (SSTs) and Sea Ice Cover (SIC) are also prescribed. Nudging data were generated from the European Centre for Medium-Range Weather Forecasts (ECMWF) Reanalysis v5 (ERA5) (Hersbach et al., 2020).

All simulations were conducted in a T42L90MA resolution with the spectral truncation T42 that translates to a $(2.7851 \times 2.8125)^{\circ}$ regular Gaussian grid in the polar regions (latitude $> \pm 68^{\circ}$ in both hemispheres). Our model setup comprises 90 hybrid pressure levels up to $0.01\,\mathrm{hPa}$. These hybrid pressure levels are terrain following, resulting in about 1–3 levels within the Arctic spring-time BL. In the Arctic, these levels translate on average to heights above ground at the upper boundary of each level as follows: level: $(1,2,3,...,8) \rightarrow \mathrm{height}: (99,254,538,...,3571)\,\mathrm{m}$.

We use the Module Efficiently Calculating the Chemistry of the Atmosphere (MECCA) (Sander et al., 2019) with the CCMI-base-02 chemistry mechanism in which mercury and iodine chemistry are switched off. This chemical mechanism comprises 261 gas-phase, 12 heterogeneous, and 80 photolysis reactions (Supplement A). The explicit calculation of heterogeneous reactions is restricted to the stratosphere and uses a prescribed aerosol surface concentration climatology (1996–2005) computed with the MESSy submodel MADE (Ackermann et al., 1998). In the troposphere and boundary layer, we parameterize the

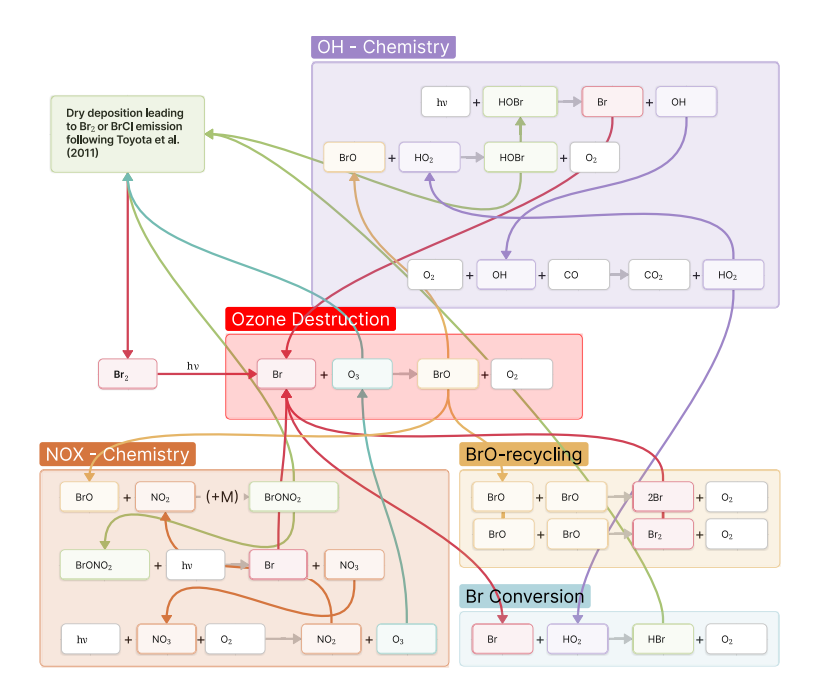


Figure 1. Schematic of bromine explosions (BEs) and catalytic ozone depletion reaction network separated by families. The emission of Br_2 and BrCl triggers the ozone destruction leading to ODEs given the availability of light for photolysis.

emission of Br_2 as described in the following paragraph. We depict the most relevant cycles for ODEs grouped by families in a reaction network (Fig. 1). The NO_x cycle can be net-zero regarding ozone destruction and production.

115

120

125

In the following, we briefly describe the most relevant MESSy submodels that handle trace gas emissions and sinks. For a complete list of submodels used in this study, please consult the file switch.nml in Supplement A (EMAC_namelists.zip). The boolean values therein indicate whether the submodels were used.

Trace gas emissions that depend on the state of the Earth system components (atmosphere, land, and ocean) are computed during the model integration in the MESSy submodel ONEMIS Kerkweg et al. (2006b). Therein, the subroutine AirSnow (Falk and Sinnhuber, 2018) handles the emission of bromine from sea ice and snow in the polar regions following the scheme suggested by Toyota et al. (2011). The dry deposition flux of O_3 on first-year sea ice (FY) triggers Br_2 emissions. Assuming that a considerable amount of bromide (Br^-) has already been pushed out of multi-year sea ice (MY), recycling is limited by the amount of inorganic bromine (HBr, BrNO₃, and HOBr) deposition from gas-phase. A similar assumption is used for snow on land (LS). The distribution of MY sea ice is prescribed. This scheme introduces a critical temperature $T_{\rm crit}$ effectively acting as a seasonal limit and a critical solar zenith angle ($\theta_{\rm crit}$) as a trigger that separates dark from sun-lit conditions with two molar yields (ϕ_1 , ϕ_2) parameterizing in-snow photochemistry. The sea salt aerosol mass flux is computed with the LSCE scheme (Guelle et al., 2001) that applies lookup tables depending on wind speed. A detailed comparison of all available sea salt aerosol emission schemes is found in Kerkweg (2005). The corresponding bromine flux is derived by scaling this flux with a Cl to Br molar ratio of 667 and assuming half of this flux is released into the gas-phase (Yang et al., 2008).

Ocean-to-atmosphere fluxes of organic substances dissolved in seawater (e.g. dimethylsulfate (DMS), bromoform $CHBr_3$ and dibromomethane CH_2Br_2) (Pozzer et al., 2006) are computed by the AIRSEA submodel. The flux for each species is calculated from concentration gradients in the uppermost ocean layer and the lowermost atmosphere layer. The species-specific Henry's law constant defines the respective solubility. The corresponding concentrations of brominated very short-lived substances (VSLS) in ocean waters are taken from Wang et al. (2019b).

The submodels OFFEMIS and TNUDGE handled emissions from preprocessed 4D forcing fields (Kerkweg et al., 2006b). Emission inventories of greenhouse gases (GHGs), Ozone Depleting Substances (ODSs), and ozone precursors are based on the German Aerospace Centre (Deutsches Zentrum für Luft- und Raumfahrt, DLR) CCMI2 inventory (available until 2019). GHGs included are N₂O, CH₄, and CO₂. ODSs include a wide range of halons, chlorofluorocarbons (CFCs), and hydrochlorofluorocarbons (HCFCs). Also included are potential ozone precursors like Volatile Organic Compounds (VOCs) and Non-Methane-Hydro-Carbons (NMHCs) from biomass and agricultural waste burning as well as in fossil fuel emissions from traffic and non-traffic consisting of VOCs (only acetylene (C₂H₂)), NMHCs, NO, CO, SO₂, NH₃ plus aerosol SO₄ derived from SO₂, organic carbon (OC) and black carbon (BC) emissions. These CCMI2 inventories are not available beyond 2019 for our model, so we substituted the missing data with 2019 emissions.

Emissions of the minor VSLS (CHCl $_2$ Br, CHCl $_2$ Br, CH $_2$ Cl $_3$ Br are based on Warwick et al. (2006). The submodel TNUDGE nudges the surface concentration climatologies of the long-lived halons CF $_3$ Br and CF $_2$ Cl $_3$ Br towards observed mixing ratios.

Dry deposition is the most important way of removing non-soluble chemical substances from the atmosphere. The corresponding dry deposition velocities ($v^{\rm dd}$) are computed by the submodel DDEP (Kerkweg et al., 2006a) following the Wesely-scheme (Wesely, 1989):

$$v^{\rm dd} = \frac{1}{r_a + r_b + r_c},\tag{1}$$

with aerodynamical resistance (r_a) driven by atmospheric turbulence, quasi-laminar resistance (r_b) driven by molecular diffusion and turbulence, and surface resistance (r_c) . For most species, there are no observations of r_c . Estimates are calculated based on the Henry's law coefficient (H_i) , a reactivity rate coefficient (R_{dry}^i) , and r_c of O_3 and sulfur dioxide (SO_2) :

$$r_{c,\text{snow}}^{i} = \frac{1}{\frac{H_{i}}{r_{c,\text{snow}}^{\text{SO}_{2}} \cdot 10^{5}} + \frac{R_{\text{dry}}^{i}}{r_{c,\text{snow}}^{\text{O}_{3}}}}$$
(2)

with $r_{c,\,{
m snow}}^{{
m O}_3}=2000\,{
m s}\,{
m m}^{-1}$ and $r_{c,\,{
m snow}}^{{
m SO}_2}=1\,{
m s}\,{
m m}^{-1}.$

Wet deposition of soluble species is calculated via the SCAV submodel (Tost et al., 2006). It considers convective and large-scale precipitation separately as well as three modes of scavenging from ice-, liquid- and gas-phase.

155 2.2 Observational data

130

135

140

150

For evaluating our model results, we use surface ozone VMR from a network of Arctic monitoring sites, satellite observations of BrO column VCD from the TROPOspheric Monitoring Instrument (TROPOMI) onboard the European Space Agency (ESA)

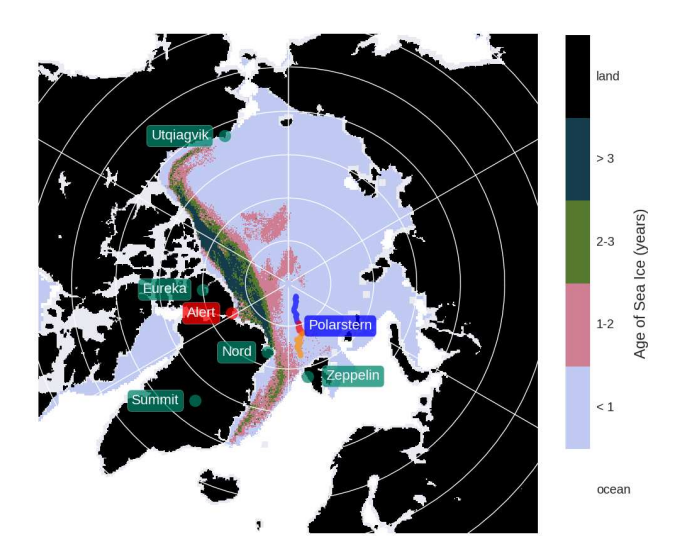


Figure 2. Locations of the Arctic ozone monitoring sites used in this work. The Research vessel Polarstern's drift track during the MOSAiC expedition (March-April-May 2020) is indicated in blue-red-orange, respectively. A spring 2020 mean sea ice age distribution from the Integrated Climate Data Center (ICDC) age of sea ice product (Tschudi et al., 2024) is shown.

Copernicus Sentinel-5 Precursor satellite, and atmosphere and trace gas observational records from the Multidisciplinary drifting Observatory for the Study of Arctic Climate (MOSAiC) expedition (2019/20). The ozone monitoring sites and MOSAiC drift track locations' are shown in Fig. 2.

2.2.1 Ozone monitoring sites

There are several monitoring sites providing long- and short-term $\chi_{\rm O_3}$ records in the Arctic as listed in Table 1. For studying the similarity between modeled and observed $\chi_{\rm O_3}$, and possible changes due to a changing climate, we use long-term data from the National Oceanic and Atmospheric Administration (NOAA) atmospheric monitoring station Barrow at Utqiaġvik, Alaska (USA) (McClure-Begley et al., 2024) spanning 5 decades, the over 3 decade long ozone record from Mt. Zeppelin, Ny-Ålesund (Spitsbergen), and almost 30 years of observations from Alert, Nunavut (Canada). We supplement these with data records from sites located at Eureka, Nunavut (Canada), and Nord and Summit both located in Greenland (Denmark). All data, except for Barrow station, have been downloaded from the EBAS website (Norsk institutt for luftforskning (NILU)) in 1-hourly resolution. All model output was interpolated to the sites' locations using the MESSy submodel SCOUT. No vertical interpolation to the stations' exact altitudes was performed.

2.2.2 TROPOMI

170

The ESA Copernicus Sentinel 5-Precursor satellite was launched in October 2017 with a designed lifetime of 7 years. It is on a sun-synchronous orbit with local time of ascending node is at 13:30 h. The TROPOMI instrument has a near-nadir resolution

Table 1. Ozone monitoring sites in the Arctic and data periods used in this work.

Station	Period	Coordinates			
		latitude longitude		altitude	
		(° N)	(° E)	(m)	
Alert [†]	1988–2013	82.499	-62.341	204.0	
Eureka ^{†,‡}	2018-2024	79.983	-85.95	610.0	
Nord †	2001-2022	81.600	-16.67	20.0	
Utqiaġvik [‡]	1973-2024	71.323	-156.611	11.0	
Summit [†]	2000-2024	72.578	-38.459	3238.0	
Mt. Zeppelin [†]	1989–2024	78.910	11.888	474.0	

Data source: † NILU - EBAS, † NOAA - Global Monitoring Laboratory. More details under *data availability*.

of $3.5 \times 7 \,\mathrm{km^2}$ ($3.5 \times 5.5 \,\mathrm{km^2}$ since July 2022) and a swath width of $2,600 \,\mathrm{km}$. Its level 2 data products include O_3 (total and tropospheric column, profile), NO_2 (total and tropospheric column), SO_2 (total column), and carbon monoxide CO (total column). For this study, PO total and tropospheric columns have been retrieved with an optimized and adapted Differential Optical Absorption Spectroscopy (DOAS) retrieval algorithm that was developed for earlier satellite missions (Seo et al., 2019, 2020). To isolate the tropospheric from the total column, a stratospheric PO climatology (Theys et al., 2009) has been used. As no total column air-mass factor (AMF) for TROPOMI is currently available, a stratospheric AMF has been applied for the total columns. For the tropospheric columns, a simplified approach was used assuming a bright surface (albedo of 0.9) and a PO surface layer of PO with thickness. This affects the retrieval over dark surfaces, e.g. ocean, and boreal forest, by reducing the amount of reconstructed PO VCD (Choi et al., 2012).

In Fig. 3 TROPOMI monthly mean BrO total and tropospheric column VCD are shown for April 2019. The tropospheric column VCD (Fig. 3(b)) indicates BrO enhancement over the whole Arctic Ocean but most prominently over the Canadian archipelago and the Kara/Laptev Sea (BrO VCD = $(3-4) \cdot 10^{13}$ molec cm⁻²).

2.2.3 MOSAiC expedition

The MOSAiC expedition was the largest scientific expedition in the Arctic to date. From September 2019 to October 2020, the German research vessel Polarstern drifted with the sea ice in the Central Arctic. In the course of this mission, a multitude of interdisciplinary experiments were conducted, including the measurement of meteorological conditions (Jozef et al., 2023) as well as O₃ (Angot et al., 2022), Br and BrO(Mahajan, 2022). The position of Polarstern during Spring 2020 is shown in Fig. 2.

The modeled surface temperature and BL height interpolated to the drift track are in general in good agreement with the observations (Fig. 4). This demonstrates that nudging with ERA5 reproduces the observed weather and meteorological conditions. Below $-10\,^{\circ}$ C, however, modeled surface temperatures becomes apparently warmer than observed (2K < $\Delta T_{\rm surf}$ < 10K)

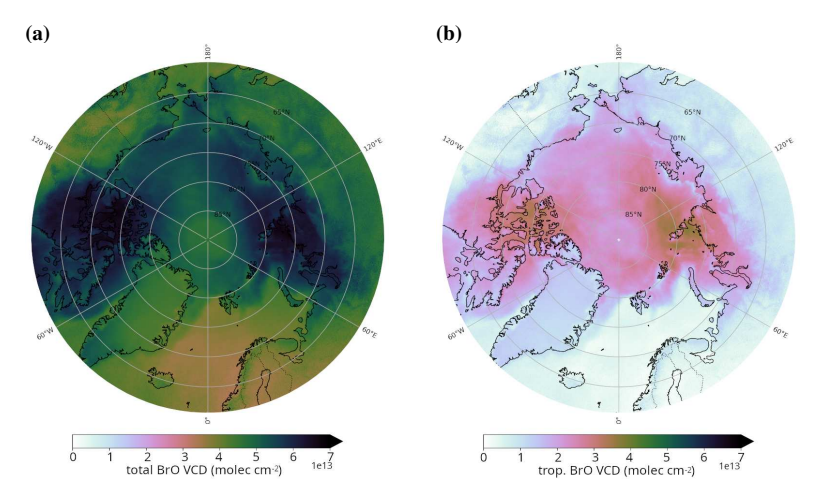


Figure 3. TROPOMI BrO VCD for April 2019. Stratospheric BrO from a stratospheric climatology by Theys et al. (2009) was subtracted from TROPOMI total column to derive the tropospheric contribution. (a) Total column; (b) Tropospheric column.

195 (Fig. 4(c)). This warm bias increases with decreasing temperatures and is most prominent when BL heights are below 100 m. This could be caused by the ERA5 nudging data in combination with the relatively low vertical model resolution in the BL. However, nudging only starts above model level 8. Wang et al. (2019a) have identified a regionally varying bias in both ERA-interim and ERA5 that increases at low temperatures (most notably below -20° C) compared with buoy observations which is similar to the bias observed in our model experiments.

3 Model parameter sensitivity and setup

200

205

In this section, we describe the sensitivity of the AirSnow algorithm to critical parameters and boundary conditions. We introduce a more realistic multi-year sea ice concentration derived from the Integrated Climate Data Center (ICDC) age of sea ice product (Sect. 3.1) and implement a sigmoidal relaxation of the temperature threshold (Sect. 3.2). We test the performance of the AirSnow algorithm and find the best model setup (Sect. 3.3). To make sure that the model is not over-tuned, we exclusively use the period January–July 2019 for improving the model skill in terms of O_3 at observation sites.

All model experiments are listed in Table 2. In contrast to the release version in MESSy v2.55.2, we include two critical bug fixes concerning the temperature (conversion from Celsius to Kelvin) and solar zenith angle (sign flip) thresholds. We have already reported and fixed these in the release candidate of MESSy v2.56.

By default, bromine prescribed from the sea salt aerosol mass flux was not treated as chemical tracer, referred to as *diagnostic* in Table 2. We refer to the inclusion of Br₂ to the tendency of the respective chemical tracer at the lowest atmospheric level as *interactive*.

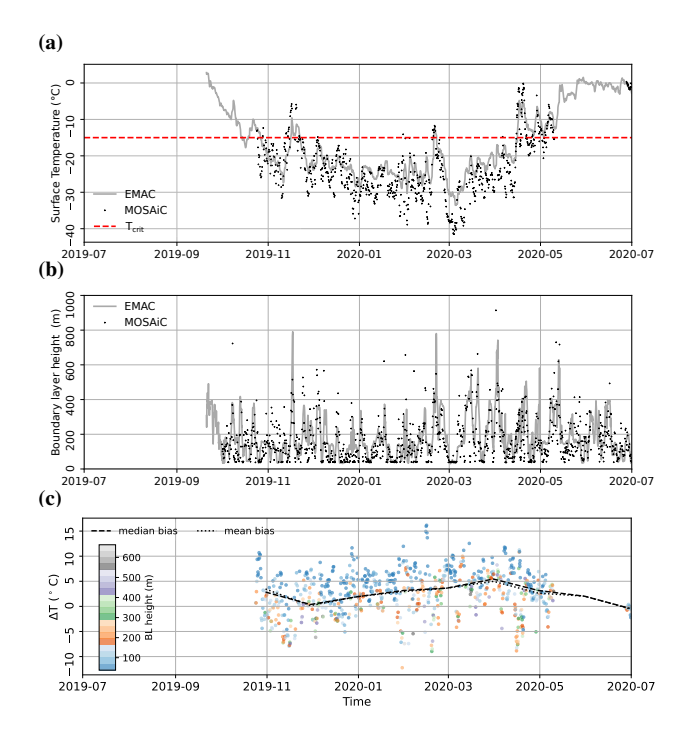


Figure 4. Comparison of meteorological observations during the MOSAiC expedition with EMAC model results from the reference simulation mapped to the MOSAiC drift track. (a) Surface temperature; (b) BL height; (c) Temperature difference ($\Delta T = T_{\rm EMAC} - T_{\rm MOSAiC}$), observed BL height indicated by color. The dashed red line represents $T_{\rm crit} = -15\,^{\circ}{\rm C}$.

Frozen freshwater lakes were originally included in the model's SIC, which caused false BEs around the Great Lakes as these were treated like first-year sea ice. We therefore, first excluded these areas by masking them out in the SIC and later treated them like land snow.

215 3.1 Multi-year sea ice cover fraction

225

By construction, the amount of Br_2 emitted using the Toyota scheme is sensitive to the assumed age of sea ice. Therefore, we expect more Br_2 emissions from regions with a large first-year sea ice concentration (FYSIC). Falk and Sinnhuber (2018) derived a multi-year sea ice concentration (MYSIC) from ERA-interim with the assumption of a static multi-year sea ice distribution computed from the SIC at the seasonal minimum of the previous year. We used the same assumption to derive MYSIC from ERA5 SIC and compared this with an age of sea ice (AoSI) product provided by the Integrated Climate Data Center (ICDC) (Tschudi et al., 2024).

ICDC AoSI uses sea ice drift data from satellite observations to assign an age to the individual ice floats for which drift trajectories are computed. Each grid cell with at least 15% SIC is treated as a Lagrangian particle and traced every week. The co-existence of ice of varying ages in one grid cell prefers the survival of the older ice because younger and thinner sea ice deforms and melts more easily. This causes an overestimation of the multi-year sea ice cover.

Table 2. List of model experiments. We use MESSy v2.55.2 including two critical bug fixes in the AirSnow mechanism that have been integrated into the MESSy release candidate. The MECCA chemistry mechanism CCMI2-base-01 has been applied for all experiments. MYSIC based on ICDC Age of Arctic Sea Ice has been made available to the MESSy community. Sea salt bromine was not treated as chemical tracer by default, here referred to as *diagnostic*. Frozen lakes are included in the model's SIC and were either masked out or treated like land snow. Experiment sfa002 has been submitted to the Arctic Bromine Model Intercomparison project.

Exp.	Period	AirSnow	MYSIC	$T_{ m crit}$	Sea salt bromine	notes
ref	2019-01-2020-07	off	-	-	diagnostic	
sfa002	2019-01-2020-07	on	ERA5	$-15^{\circ}\mathrm{C}$	diagnostic	model intercomp.
sfa008	2019-01-2019-07	on	ERA5	$-15^{\circ}\mathrm{C}$	diagnostic	+ frozen lakes masked
						+ sigmoidal $T_{ m crit}$
sfa010	2019-01-2019-07	on	ICDC	$-15^{\circ}\mathrm{C}$	diagnostic	+ frozen lakes masked
						+ sigmoidal $T_{ m crit}$
sfa011	2019-01-2019-07	on	ICDC	$-10^{\circ}\mathrm{C}$	diagnostic	+ frozen lakes masked
						+ sigmoidal $T_{ m crit}$
sfa012	2019-01-2019-07	on	ICDC	$-2.5^{\circ}\mathrm{C}$	diagnostic	+ frozen lakes masked
						+ sigmoidal $T_{ m crit}$
sfa013	2019-01-2019-07	on	ICDC	$-10^{\circ}\mathrm{C}$	diagnostic	+ frozen lakes like LS
						+ sigmoidal $T_{ m crit}$
sfa017	2019-01-2020-07	on	ICDC	$-10^{\circ}\mathrm{C}$	interactive	+ frozen lakes like LS
						+ sigmoidal $T_{ m crit}$

To derive a MYSIC, we summed over all ICDC age classes $\geq 1\,\mathrm{year}$ and average the bi-weekly data over one month. The original resolution of $12.5 \times 12.5\,\mathrm{km}$ was then remapped onto the target resolution (e.g. T42, T106, Appendix Fig A1).

Compared to ERA5-derived MYSIC, ICDC AoSI indicates distinctively less multi-year sea ice in the Central Arctic Ocean and the Canadian archipelago but more east of Greenland, north of Spitsbergen and Alaska (Fig. 5(a)). To identify which of the two MYSIC estimate is more realistic, we computed the total area covered by multi-year sea ice. The area derived from ERA5 is consistently $\sim 30\%$ larger than from ICDC AoSI over the period 1980 to 2020 (Appendix Fig. A2(a)). The total area of multi-year sea ice based on ICDC AoSI amounts on average to $2.5 \cdot 10^6 \, \mathrm{km}^2$ in the 2020s, which is consistent with the range $(0.5-2.9) \cdot 10^6 \, \mathrm{km}^2$ given by Regan et al. (2023) for the time period 2009–2019.

230

235

We conducted two model experiments that differ only in the applied MYSIC (ERA5, ICDC AoSI) and found that the lower the MYSIC in a grid cell the more Br_2 and the less BrCl emissions from ice and snow are simulated (Fig. 5(b)). The opposite is true for grid cells with larger MYSIC. This means that strong local sources of Br_2 due to small-scale sea ice inhomogeneities may appear smeared out in our applied model resolution.

For our model experiments, we computed BrO VCD from $\chi_{\rm BrO}$ and used a dynamical tropopause metric based on the model potential vorticity (PV) at $3.5\,\rm PVU$ ($1\,\rm PVU=10^{-6}\,m^2\,s^{-1}\,K\,kg^{-1}$) to separate tropospheric and stratospheric columns. We

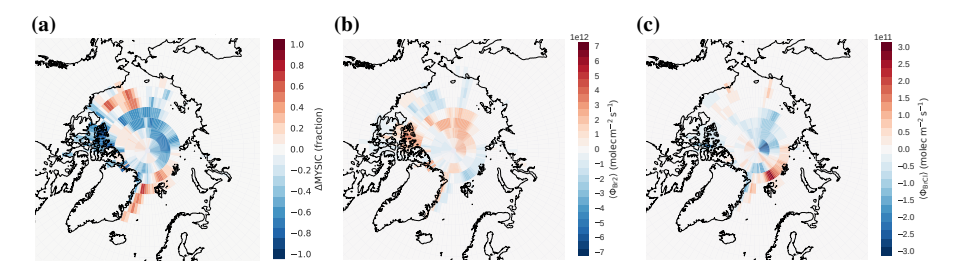


Figure 5. Influence of MYSIC on AirSnow emission fluxes. (a) MYSIC difference ICDC AoSI-ERA5. (b) Br_2 and (c) BrCl flux difference between a model experiments with ICDC AoSI (sfa010) and ERA5 (sfa008).

sampled the modeled total and tropospheric VCD at $13-14\mathrm{h}$ local time and calculated monthly averages to compare with the satellite retrieval. The mean modeled stratospheric contribution to the total BrO VCD in April was rather uniform in all experiments and amounts to $(2.5-3)\cdot 10^{13}\,\mathrm{molec\,cm^{-2}}$ (Appendix Fig. B3).

The TROPOMI BrO VCD for April 2019 (Fig. 3(a, b)) indicates hotspot regions over the Canadian archipelago and the Kara/Laptev Sea. This pattern is well reproduced in experiments with ICDC AoSI-derived MYSIC (Appendix Fig. B4(c, d)). The ERA5-derived MYSIC shows an additional hotspot at the Alaskan coast (Appendix Fig. B4(a, b)) which is absent in the satellite VCD. Therefore, we conclude that MYSIC derived from ICDC AoSI is the better choice.

3.2 Temperature threshold

245

250

260

The threshold temperature $T_{\rm crit}$ constrains the occurrences of BEs in time and space during the spring. Toyota et al. (2011) noted that there is no $T_{\rm crit}$ that optimizes modeled ozone at all monitoring sites simultaneously. We propose that relaxing this temperature threshold might improve the agreement without implementing a detailed snow microphysics and snow chemistry scheme (Toyota et al., 2014) in a global CCM. For this purpose, we implemented a sigmoidal temperature dependency of the form

$$f_{\text{crit}}(T) = \frac{1}{1 + e^{T - T_{\text{crit}}}},\tag{3}$$

with T the surface temperature in a given grid cell. The Br_2 and BrCl emission fluxes are then scaled with $f_{\mathrm{crit}}(T)$ and reach 10% and 90% of the maximum flux at $T_{\mathrm{crit}} \pm 2.2\,^{\circ}\mathrm{C}$, respectively. Br_2 emissions thus already increase where temperatures are slightly above T_{crit} , most notably in coastal regions.

We then looked at model results at $T_{\rm crit} \in \{-15, -10, -2.5\}$ °C. $T_{\rm crit} = -2.5$ °C means allowing bromine emission also at temperatures around the freezing point of freshwater. With a higher threshold temperature, the modeled Br_2 fluxes consistently show an increase over first-year sea ice (Fig. 6(d, g)). Emissions from multi-year sea ice regions, indicated by the BrCl fluxes (Fig. 6(c, h)), also display an increase but remain two orders of magnitude lower than emissions from first-year sea ice

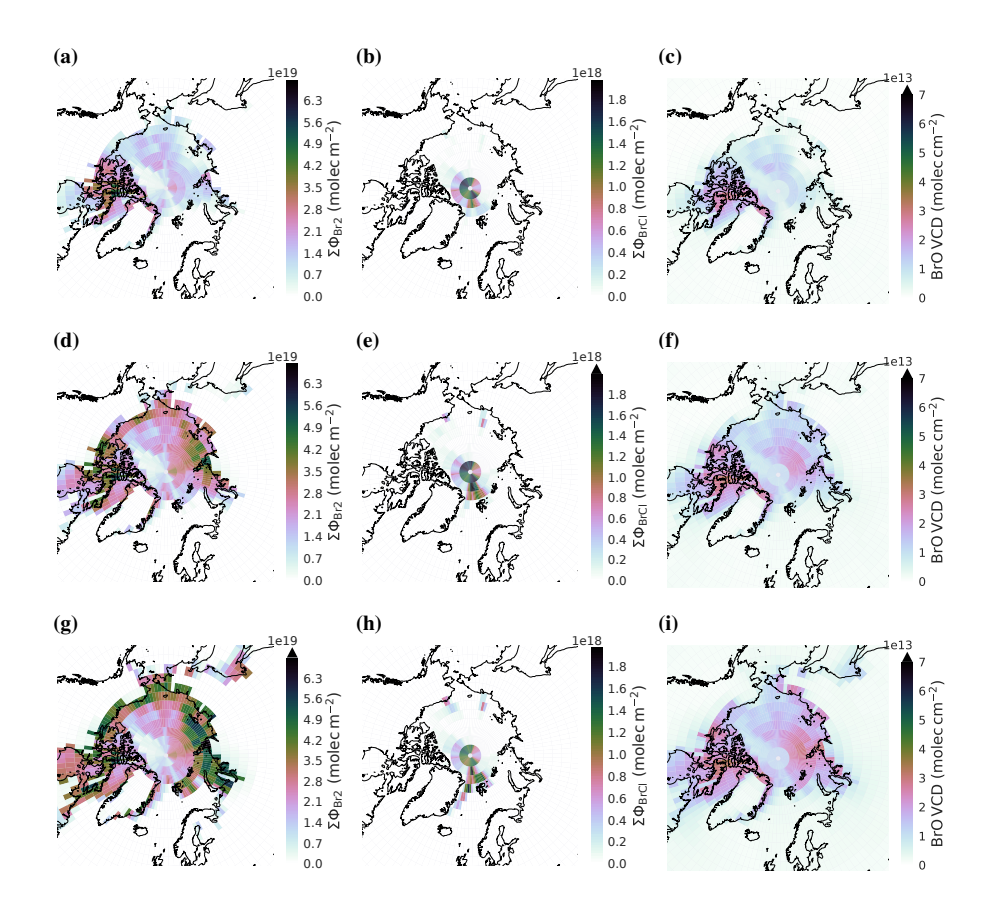


Figure 6. Comparison of modeled bromine emissions due to BEs and tropospheric BrO VCD. Flux integral of (a, d, g) Br₂ and (b, e, h) BrCl and monthly mean tropospheric BrO VCD at $13-14\,\mathrm{h}$ local time (c, f, i) for April 2019. The EMAC total column BrO has been split into tropospheric and stratospheric contributions using the modeled PV-tropopause height on hourly basis. (a–c) $T_{\rm crit}=-15\,^{\circ}\,\mathrm{C}$ (sfa010); (d–f) $T_{\rm crit}=-10\,^{\circ}\,\mathrm{C}$ (sfa011); (g–i) $T_{\rm crit}=-2.5\,^{\circ}\,\mathrm{C}$ (sfa012).

regardless of the choice of $T_{\rm crit}$. At $T_{\rm crit} = -2.5\,^{\circ}{\rm C}$, the model predicts ${\rm Br}_2$ emissions in the Gulf of Bothnia, the White Sea, and the Sea of Okhotsk (Fig. 6(g)), though this does not result in notably enhanced ${\rm BrO~VCD}$ (Fig.6(i)).

At $T_{\rm crit}=-2.5\,^{\circ}{\rm C}$ the BrO VCD in the hot spot regions is closest to the TROPOMI VCD (Fig. 3(b)), though more enhanced BrO VCDs are found at the coast east of Greenland and East Siberia than observed. As indicated above, this could be a relict of the relatively low model resolution and associated land-sea mask that does not resolve all topographic features and congruent sub-grid temperature variance. Possibly, the stratospheric BrO climatology and simple AMF used in the TROPOMI retrieval also plays a role for the absolute values. Overall, our modeled BrO VCD in 2019 agrees best with satellite observations (Fig. 3(b)) in both amount and spatial pattern of tropospheric BrO VCD at $T_{\rm crit}=-2.5\,^{\circ}{\rm C}$.

3.3 Model skill and best setup

To decide on the best model setup, we evaluated the model skill in terms of the coefficient of determination of the linear regression (squared Pearson correlation coefficient, R^2) and root-mean-square-error (RMSE) at the Arctic ozone monitoring sites (Sect. 2.2.1) for spring 2019.

The resulting R^2 and RMSE for 2019 at Utqiagvik, Eureka, Summit, and Zeppelin are listed in Table A1. The closer R^2 is to 1, the better the correlation. The closer the RMSE is to 0, the smaller the difference between the observed and modeled time series. For the corresponding histograms with fitted linear regression curves, see Appendix Fig. A4.

We confirmed that there is not a single combination of parameters that optimizes both R^2 and RMSE for all sites. The model experiment with MYSIC from ICDC AoSI and $T_{\rm crit}=-15\,^{\circ}{\rm C}$ (sfa010) performs best with respect to R^2 ($\langle R^2 \rangle = 0.198$). The experiments with $T_{\rm crit}=-10\,^{\circ}{\rm C}$ (sfa011, sfa017) are best in terms of RSME ($\langle {\rm RMSE} \rangle = 0.365$). The treatment of freshwater lakes like land snow decreases the model skill slightly compared to the experiments where these are excluded (compare (sfa013, sfa017) with (sfa010, sfa011)). We will need to investigate this further. An experiment (sfa012) with $T_{\rm crit}=-2.5\,^{\circ}{\rm C}$ performs well at Zeppelin, but displayed lower modeled $\chi_{\rm O_3}$ than observed at Eureka and Villum research station Nord in May and June (Appendix Fig. B2). At higher spatial resolution ($15\times15\,{\rm km}$), Gong et al. (2025) have shown that, when using an ODE terminator defined by snowmelt and additional bromine emission from multi-year sea ice, observed and modeled $T_{\rm crit}=-2.5\,^{\circ}{\rm C}$, but was underestimated at Villum research station Nord. This suggests that BEs near Zeppelin may persist at relatively high temperatures as compared to other ice-covered regions for unidentified reasons.

Based on these quantitative results, we decided on the setup with MYSIC derived from ICDC AoSI, $T_{\rm crit} = -10\,^{\circ}{\rm C}$, and ${\rm Br_2}$ emissions from sea salt enabled (sfa017). As stated above, tropospheric BrO VCD showed a qualitatively better agreement with $T_{\rm crit} = -2.5\,^{\circ}{\rm C}$.

4 Results

275

280

Our special focus lies on the spring 2020 for which ozone monitoring station records, TROPOMI satellite observations, and data from the MOSAiC expedition are available. In this section, we show the surface ozone VMR time series at different sites for our best model setup and compute probability density functions (PDFs) of χ_{O3} from observation and model results to look for indications of a possible climate change impact on ODEs (Sect. 4.1). We use the MOSAiC data to judge the overall model skill in the Central Arctic qualitatively (Sect. 4.2) and compare the modeled pan-Arctic pattern of ozone depletion and BrO VCD with TROPOMI retrieved BrO VCD (Sect. 4.3).

4.1 Arctic ozone monitoring sites

4.1.1 Ozone time series 2019/20

For the Arctic ozone monitoring sites Eureka, Nord, Summit, Utqiagʻvik, and Zeppelin, we show the 2019/20 composite time series of modeled (ref, sfa017) and observed χ_{O_3} in Fig. 7. We find that the effect of AirSnow on ozone VMR is confined

temporally. As soon as the trigger conditions for ODEs are not satisfied anymore, O₃ VMR returns quickly to the values of the reference simulation. It is evident that AirSnow qualitatively improves the EMAC model capabilities of capturing tropospheric ozone in the Arctic spring at all sites. Key features like the late April to early May ODE in 2019 at Eureka and Utqiaġvik and the late March to late April ODEs at Utqiaġvik in 2019 match reasonably well in their timing but not in the observed strength of the ozone depletion. An ODE in March 2019 at Eureka station coinciding with a pronounced dip in ozone at Summit is not reproduced. The EMAC model generally underestimates χ_{O3} in Arctic winter. Following Helmig et al. (2007), Falk and Sinnhuber (2018) have shown that a higher surface resistance of ozone over ice and snow (r_c = 10000 sm⁻¹) could improve this. In 2020, especially in March and May, ODEs at Eureka and Utqiaġvik were captured less well, also reflected by a reduced model skill compared to 2019 (see Tab. B1). This was potentially caused by the recycling of 2019 emission inventories. As a secondary pollutant, tropospheric ozone depends on precursor substances like NO_x, CO, and VOCs. COVID-19 policies reduced their emissions which had a measurable effect on tropospheric ozone (Weber et al., 2020; Venter et al., 2020; Steinbrecht et al., 2021).

Beyond Arctic springtime, we found peak ozone VMR at Utqiagʻvik in June 2019 and 2020 that are much larger than observed. These peak values are likely caused by large wildfires raging within the Arctic circle in 2019 (Descals et al., 2022). These usually contribute to ozone precursors and cause episodes of enhanced tropospheric ozone (Cofer et al., 1990; Lindskog et al., 2007; Karlsson et al., 2013). However, Baker et al. (2016) have reported that attenuation of solar radiation and aging of aerosols are potentially underestimated in chemistry transport models causing photolyis rates and therefore in situ ozone production to be overestimated compared to observations. For reference, surface ozone time series including only the bug fixes are shown in Appendix Fig. B1.

4.1.2 Ozone climatology

315

330

We assume that the amount of Br₂ emitted and, subsequently, the strength of ODEs should be highest for a high FYSIC (Falk and Sinnhuber, 2018). Around 2007, the amount of multi-year sea ice in the Arctic prominently dropped (Regan et al., 2023) (Appendix Fig. A2). Hence, we would expect an increased occurrence of ODEs after 2007. To test this hypothesis, we divided the observational datasets with long-term records into two periods: (1) start of record until the end of 2007 and (2) 2008 until the end of each record. For these two periods, we computed PDFs of observed χ_{O3} as normalized histograms with 1 ppbv
binning (Fig. 8). The Arctic ozone monitoring sites with long-term records are Alert, Utqiaġvik, and Zeppelin. Error bars denote the year-by-year variance of the observational data using standard deviation.

In March, observations at Alert and Zeppelin display close-to-normal distributions peaking between $40-45\,\mathrm{ppbv}$ with a small tail towards low $\chi_{\mathrm{O_3}}$. These tails become larger throughout April and May and transform the distribution into a close-to-equal distribution which can be interpreted as an ODE fingerprint. The distribution at Utqiaġvik shifts to a close-to-equal distribution already in March owing to its more southern location. The close-to-equal distribution of $\mathrm{O_3}$ VMR during the ODE season is in line with previously identified temporally varying frequency distributions of $\chi_{\mathrm{O_3}}$ in ship (Jacobi et al., 2010) and airplane (Ridley et al., 2003) expeditions in the Central Arctic.

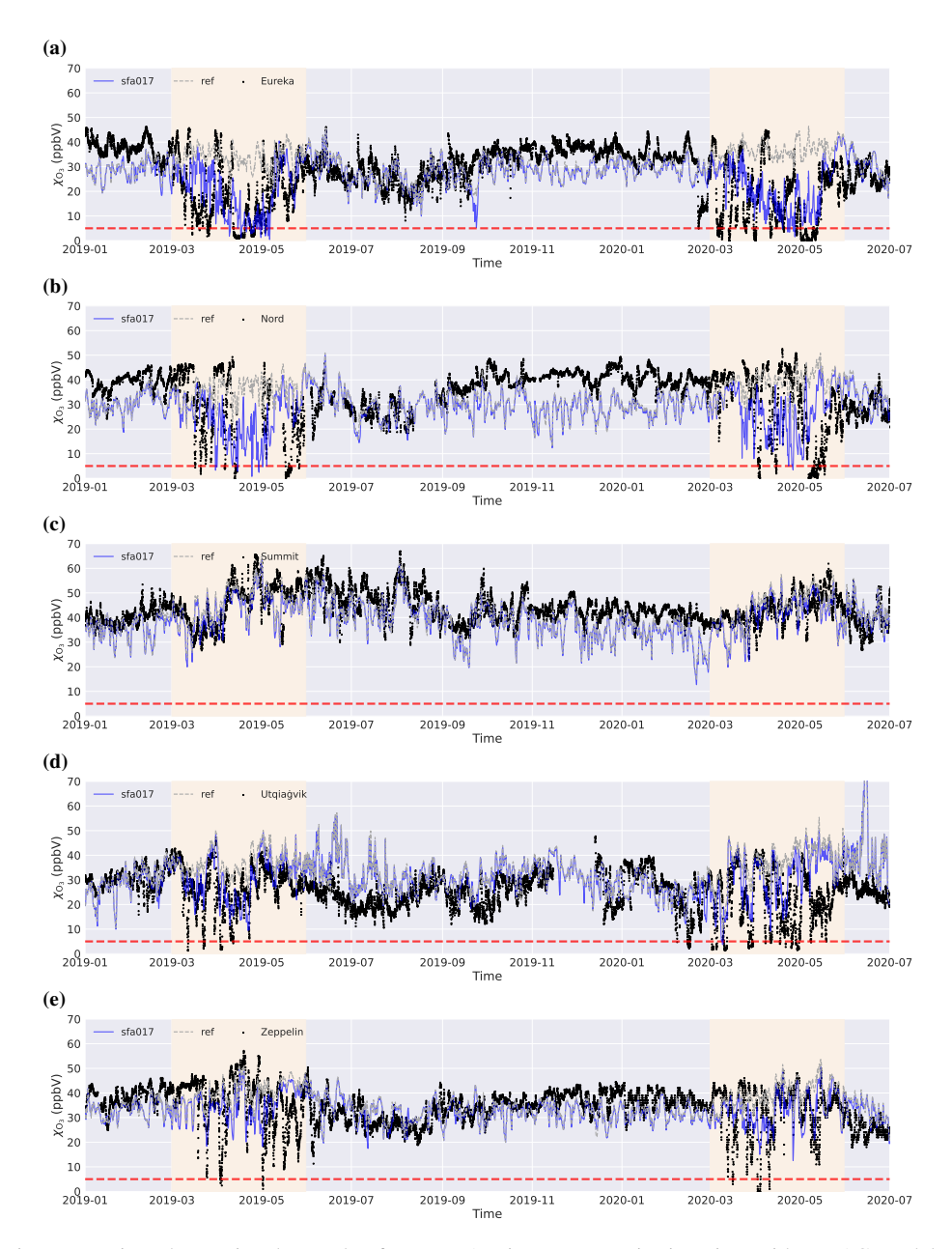


Figure 7. Time series comparing observational records of χ_{O_3} at Arctic ozone monitoring sites with EMAC model output (ref, sfa017) interpolated to the station location. The periods March–May are highlighted in light yellow. The dashed red line indicates the 5 ppbv threshold for ODEs. (a) Eureka; (b) Nord; (c) Summit; (d) Utqiagʻvik; (e) Zeppelin.

In the observational period (2), all sites' distributions display a significant increase of higher χ_{O_3} compared to period (1) in spring. In period (2) data at Utqiagvik show the onset of a return to a close-to-normal distribution already in May compared to period (1). This means that conditions became less favorable for ODEs in recent decades. In April and May, the ODE

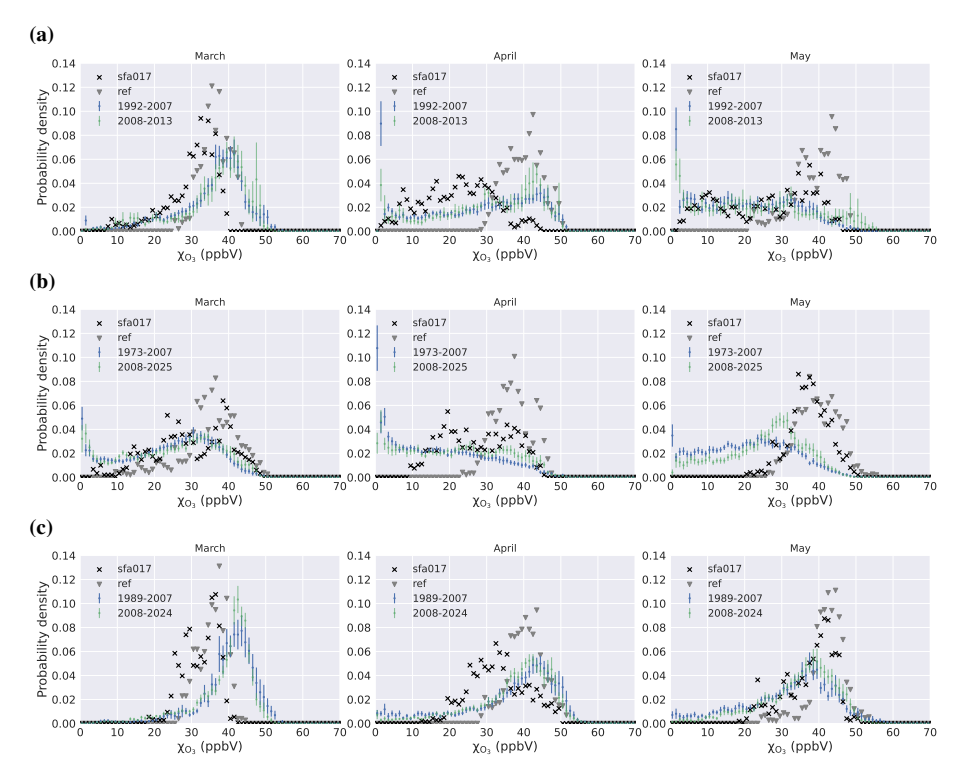


Figure 8. Histogram of χ_{O_3} for EMAC experiments sfa017 and ref (2019/20) compared to long-term observations separated into two periods: start of record to the end of 2007 and 2008 to end of record. (a) Alert; (b) Utqiagvik; (c) Zeppelin.

bins $(\chi_{O_3} \le 10 \,\mathrm{ppbv})$ at all stations are significantly (more than 1σ) less populated in time period (2). Especially, at Zeppelin almost no ODEs occur in period (2) while atmospheric background O_3 concentrations apparently have increased. Although the instrumental uncertainty in earlier years is usually larger, these data imply a significantly less frequent occurrence of strong or continuous ODEs in recent decades. This means that either the role of bromine emissions from FYSIC in promoting ODEs is overstated, or that other climate-sensitive factors are counteracting the observed increase in BrO VCD (Bougoudis et al., 2020) in terms of ozone depletion.

The modeled distributions differ from observations beyond the expected year-to-year variance. The reference simulation follows a normal distribution for almost all sites and months. Only at Utqiagvik in March a slight tendency towards an equal distribution can be found. While generally too high, $\chi_{\rm O_3}$ at Zeppelin is too low in March. Using AirSnow, the distributions get closer to observations for some months and sites. The best agreement is achieved at Alert and Zeppelin in April and Utqiagvik in March. However, a general shift towards lower ozone at all locations leads to an underestimation of the frequency of $\chi_{\rm O_3}$ becoming greater than 37 ppbv. In March, there is only little change at Alert, Utqiagvik, and Zeppelin. In May, the PDF for Alert shifts towards lower values and is more equally distributed. We conclude that $\chi_{\rm O_3}$ distributions are captured more correctly, when accounting for the bromine emissions from ice and snow.

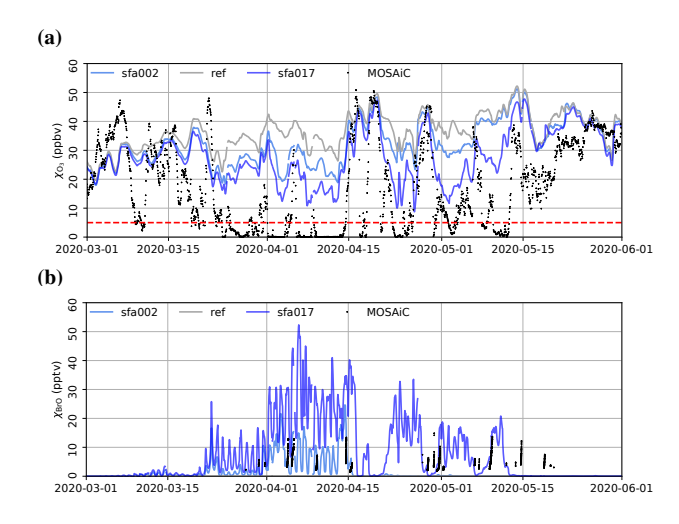


Figure 9. Evaluation of EMAC experiments (ref, sfa002, sfa017) interpolated onto MOSAiC drift track. Compared to MOSAiC observations. (a) O₃; (b) BrO. Note that $\chi_{\rm BrO}$ were not present in the reference experiment.

4.2 Ozone and bromine monoxide in the Central Arctic

In Sect. 2.2.3, we found that modeled surface temperature and BL agree reasonably well with observations during the MOSAiC expedition. In the following, we will compare modeled χ_{O_3} and χ_{BrO} with in situ observations during the MOSAiC expedition for the leg March–May 2020.

We interpolated $\chi_{\rm O_3}$ and $\chi_{\rm BrO}$ for the model experiments ref, sfa002, and sfa017 onto the MOSAiC drift track and compared these with observations (Fig. 9). We found an ozone depletion of up to 20 ppbv with our best setup (sfa017), though the observed ODEs ($\chi_{\rm O_3} \leq 5\,{\rm ppbv}$) in the Central Arctic are not reproduced in any of our model experiments. During the modeled partial ODEs in April, much more surface BrO is produced than observed, while tropospheric BrO VCD remains lower than observed (compare Figs. 10(b,d)). In May, $\chi_{\rm BrO}$ is better reproduced, while $\chi_{\rm O_3}$ remains too high.

The photochemical steady state between Br and BrO requires the presence of O_3 to maintain BrO production (Fig. 1) (Hausmann and Platt, 1994; Zhao et al., 2016). As the ozone depletion on pan-Arctic scale remains incomplete in our model experiments, the enhanced $\chi_{\rm BrO}$ at the surface is probably a direct consequence.

4.3 Pan-Arctic implications

350

355

360

365

The pattern of observed and modeled BEs show a considerable year-by-year variability. In 2020, TROPOMI tropospheric BrO VCD displays an extended area of increased BrO from the northern tip of the Canadian archipelago to the Laptev Sea (BrO VCD $\geq 4 \cdot 10^{13}$ molec cm⁻²). In the model experiment, this region decomposes into three hotspots: the northern tip of Greenland and the Canadian archipelago (BrO VCD = $(2.5-4) \cdot 10^{13}$ molec cm⁻²), north of the Beaufort Sea, and the Laptev/Kara Sea, north of Novaya Zemliya, (BrO VCD = $(0.5-1.5) \cdot 10^{13}$ molec cm⁻²) respectively. A modeled corridor of lower BrO enhancement coincides with the maximum of MYSIC. This implies a need to reconsider the assumptions regarding

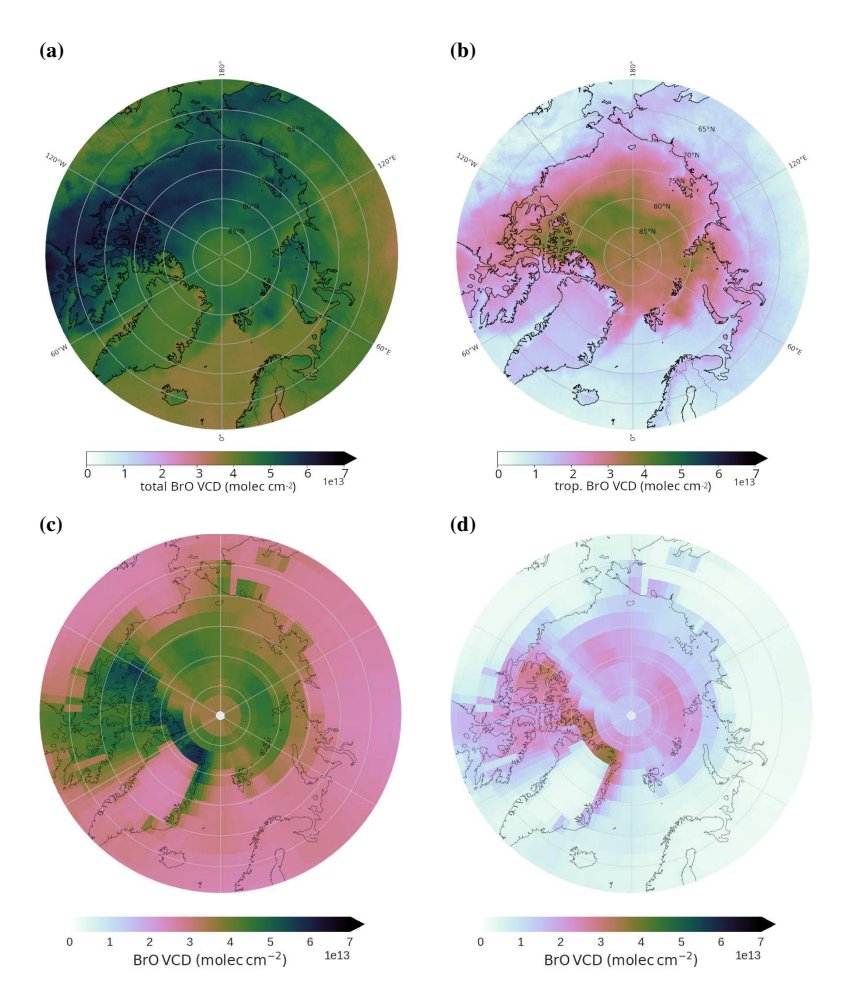


Figure 10. Monthly mean BrO VCD at 13 – 14h local time in April 2020. The EMAC total column BrO has been split into tropospheric and stratospheric contributions using the modeled tropopause height on hourly basis. A stratospheric climatology (Theys et al., 2009) was subtracted from TROPOMI total column. (a) TROPOMI (total column); (b) TROPOMI (tropospheric column); (c) sfa017 (total column); (d) sfa017 (tropospheric column).

bromine recycling on multi-year sea ice. These findings support the conclusions of Peterson et al. (2019), indicating that regions covered by multi-year sea ice serve as a more significant source of reactive bromine than previously recognized. The modeled $BrO\ VCDs$ are up to a factor of four lower than observed. As shown in Sect. 3, these scale with the amount of Br_2 emitted.

370

375

The monthly maximum of the difference in surface ozone (Fig. 11(a)) displays major hotspots ($\Delta O_{3_{max}} = (30-40)\,\mathrm{ppbv}$) in the Canadian archipelago/Baffin Bay/north of Greenland and the Laptev Sea/Eastern Arctic Ocean. These hotspots of ozone depletion colocate partly with regions of high BrO VCD (Fig. 10(d)). Ozone depletion on a pan-Arctic scale appears relatively weak on a monthly average (Fig. 11(b)) and never exceeds 17 ppbv in April compared to an ozone background of $(29\pm8)\,\mathrm{ppbv}$. Hence, modeled surface ozone is only depleted by $60\pm3\,\%$ on average. This strongly suggests that ozone depletion is too weak

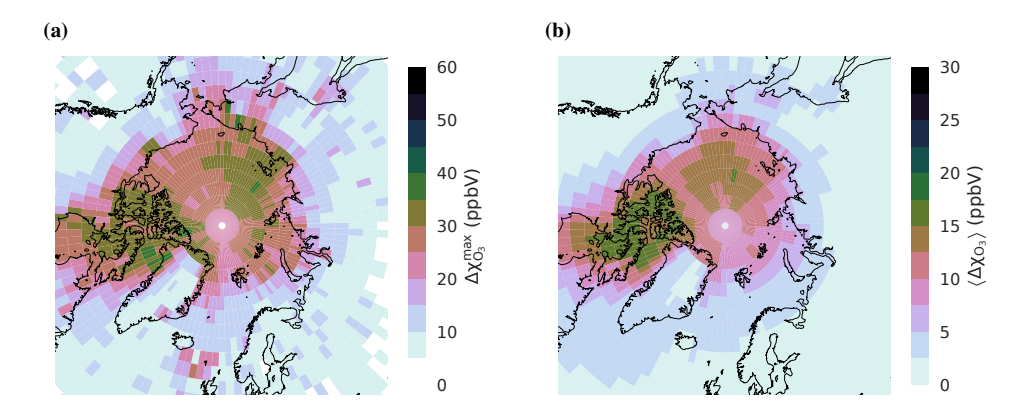


Figure 11. Monthly (a) maximum and (b) mean ozone depletion in April 2020 computed from difference between experiment sfa017 and the reference simulation.

not only along the MOSAiC drift track (Sect. 4.2) but also on larger scales. The hotspots of maximum depletion are located in the Canadian archipelago and the Central Arctic (North of the Aleutian Islands). In March and May, the major hotspot region is again located in the Canadian archipelago, while the secondary hotspots vary both in strength and location (Appendix Fig. B5).

In the mid-latitudes, an average ozone reduction of $0-5\,\mathrm{ppbv}$ compared to the reference simulation is predicted. This average ozone reduction could be due to an advection of ozone depleted as well as bromine enriched air masses from the Arctic. In this regard, we found a pronounced reduction maximum of ozone of up to $25\,\mathrm{ppbv}$ in the North Atlantic between Iceland and the Faroe Islands. This signal is colocated with prescribed shipping emissions of CO, NOx, NH₃, and SO₂ in that area and indicates that chemical ozone depletion could be locally enhanced by advected bromine from the Arctic (Fernandez et al., 2024).

5 Discussion

380

385

390

395

As a secondary pollutant, tropospheric ozone depends on precursor substances like NO_x , CO, and VOCs. COVID-19 policies reduced emissions of these which had a measurable effect on tropospheric ozone background (Weber et al., 2020; Venter et al., 2020; Steinbrecht et al., 2021). This likely affected our results for 2020, because the photochemical steady state between Br and BrO requires the presence of O_3 to maintain BrO production (Hausmann and Platt, 1994; Zhao et al., 2016). The apparently weak colocation of O_3 depletion and enhanced BrO VCD would then be a consequence of different phases of non-linear temporal evolutions in the O_3 and BrO concentrations in air masses being transported under the influence of the chemistry that leads to BEs and ODEs (e.g. Hausmann and Platt, 1994). This also fits well to airborne observations that reported no or little ozone depletion in regions with enhanced BrO VCD (Ridley et al., 2003; Salawitch et al., 2010).

Toyota et al. (2014) have demonstrated in a modeling study that snow photochemistry in the photic zone, which is leading to the formation of HOBr, contributes more to Br_2 emissions than reactions in the snow skin layer. Following these results, Zhai

et al. (2023) suggested parameterizing emissions from deeper snow layers in dependency of the solar zenith angle and showed that these emissions are important to interpret bromide records in Greenlandic ice cores. Such emissions are currently neglected in our model. Beside the parameterization of snow photochemistry, Zhai et al. (2023) also introduced a more physically oriented criterion relating snow albedo and snowmelt adapted by Gong et al. (2025) allowing for a $T_{\rm crit}=-2.5\,^{\circ}{\rm C}$. Snowmelt probably is the final terminator of BEs (Burd et al., 2017), but experiments have shown that snow-metamorphism under non-melting temperature gradients already reduces the emission potential of bromine from snow (Edebeli et al., 2020). Peterson et al. (2019) concluded, that regions covered by multi-year sea ice serve as a more significant source of reactive bromine than previously recognized. This suggests that the assumptions of an infinite bromide source and instantaneous recycling may need to be revised. Including a multi-layer snow model with snow metamorphism and explicit snow chemistry could potentially improve the prediction of the bromine emission.

For modelling the removal of trace gases from the atmosphere, dry and wet deposition processes are essential. Conceptually, the associated dry deposition resistances parameterize the uptake of trace gases on different surfaces (Wesely, 1989). Therefore, dry deposition has to be reevaluated when surface reactions are explicitly included or parameterized. For ozone, Barten et al. (2023) reported a high median dry deposition resistance ($r_c \propto 20000\,\mathrm{sm}^{-1}$) over the Central Arctic sea ice which is one order of magnitude larger than what we applied in our simulations ($r_c = 2000\,\mathrm{sm}^{-1}$). Following Helmig et al. (2007), Falk and Sinnhuber (2018) had shown an improved agreement of ozone VMR between model (MESSy v2.52) and observation for $r_c = 10000\,\mathrm{sm}^{-1}$. As shown by (Luhar et al., 2018; Pound et al., 2020), dry deposition to the ocean can be improved by considering iodine reactions and emission from the upper ocean layer. In addition, Benavent et al. (2022) have shown the importance of iodine chemistry on the loss of tropospheric ozone during the MOSAiC campaign.

Photochemistry could be underestimated in twilight conditions above surfaces with high albedo, as j-values are usually only computed for $\theta_{\odot} \leq 87^{\circ}$. For a relatively low surface albedo of 0.3, Lary and McQuaid (1991) had shown that multi-scattering at $80^{\circ} \leq \theta_{\odot} \leq 100^{\circ}$ is non-negligible even for stratospheric NO_x and O_3 chemistry. At Halley station (Antarctica), the observed ratio of upwelling to downwelling flux for j-values of selected molecules averaged 0.98 under cloudy conditions, regardless of wavelength or solar zenith angle. Under less cloudy conditions, this ratio increased with wavelength when the solar zenith angle exceeded 75° (Jones et al., 2008). At the same time, modeled surface albedo could be underestimated over sea ice with little snow cover. At a snow depth of $\geq 1\,\mathrm{cm}$ and for $T < -1\,^{\circ}\mathrm{C}$ the surface albedo is set to 0.8 in our model while for bare sea ice it is set to 0.75. In comparison, measurements by Carns et al. (2015) indicated an albedo of \sim 0.8 in the visible wavelength range on a thin, \sim 0.3 cm, crust of salty snow.

6 Summary and conclusions

400

405

410

415

420

425

We used the chemistry-climate model ECHAM/MESSy v2.55.2 nudged with ERA5 data to study ozone depletion and bromine explosions in the Arctic in spring 2019/20. We compared model predictions with observations from ozone monitoring sites, TROPOMI satellite BrO VCD, and meteorological and atmospheric tracer data taken during the MOSAiC expedition.

We improved our model setup by including a more realistic multi-year sea ice cover based on the ICDC age of sea ice product and a sigmoidal relaxation of the temperature threshold for bromine release from first-year sea ice. These changes led to a qualitative improvement between modeled and observed patterns of enhanced tropospheric BrO VCD. A temperature threshold of $T_{\rm crit} = -10\,^{\circ}{\rm C}$ improved R^2 and RMSE of ozone VMR for the ozone monitoring sites at the Arctic coast (Eureka, Utqiagvik). A threshold temperature of $T_{\rm crit} = -2.5\,^{\circ}{\rm C}$ was most favorable for the monitoring site at Mt. Zeppelin and the BrO VCD enhancement, but caused much lower modeled $\chi_{\rm O_3}$ than observed at Eureka and Villum research station Nord in May and June. Even with a sigmoidal relaxation, there exist not a single temperature threshold that improves ODEs and BrO VCD at all sites at the same time. Quantitatively, we found a weaker correlation between modeled and observed $\chi_{\rm O_3}$ at the Arctic ozone monitoring sites in 2020 compared to 2019.

430

435

440

445

455

460

By separating tropospheric and stratospheric BrO VCD at the modeled tropopause instead of subtracting a stratospheric BrO climatology, we showed that the increase in BrO VCD is defined by the modeled strength of BEs in the troposphere. Qualitatively, the spatial colocation between modeled monthly mean tropospheric BrO VCDs and the maximum ozone depletion appeared to be weaker in the Eastern Arctic than in the Canadian archipelago.

In contrast to observations, only partial ODEs ($(5 \le \chi_{O_3} \le 20)$ ppbv) could be simulated for the MOSAiC expedition's leg in March–May 2020. The modeled BrO surface VMR was much higher than observed in April, while modeled BrO VCD was lower than observed as a probable, direct consequence of the incomplete O_3 depletion. The MOSAiC atmospheric data also revealed that the modeled boundary layer height was underestimated in periods of observed shallow BL ($\le 100 \,\mathrm{m}$). During these periods, the difference in observed and modeled surface temperatures was most prominent. Observed surface temperatures below $-10\,^{\circ}\mathrm{C}$ appeared $2-10\,\mathrm{K}$ warmer in our model compared to observations.

On a long-term perspective, Arctic sea ice age, extent, and thickness have been decreasing strongly in the recent decades. This decrease should cause an increase in the occurrence of ODEs and BEs if first-year sea ice was the major driver. However, the Arctic ozone monitoring stations with the longest records (Alert, Utqiagʻvik, and Zeppelin) showed a significant decrease in the probability of $\chi_{O_3} \leq 5$ ppbv post year 2007. At the same time, the probability to observe higher χ_{O_3} increased. These data imply a significantly less frequent occurrence of strong or continuous ODEs in recent decades. This suggests that the role of bromine emissions from FYSIC in promoting ODEs may be overstated, or that other climate-sensitive factors are counteracting the observed increase in BrO VCD (Bougoudis et al., 2020) in terms of ozone depletion. Model integration over several decades could be useful to identify the factors contributing to BEs and ODEs that are linked to climate change.

We further need to investigate the contributions of neglected processes like sea salt aerosols from blowing snow, missing chemical pathways including iodine chemistry, and multiphase chemistry on sea salt aerosols in the Arctic marine boundary layer.

To conclude, several key areas should be explored to advance our understanding of ozone and bromine chemistry in the Arctic. First, contributions of bromide distribution in deeper snow layers to bromine emissions and snow metamorphism should be considered, as they play a crucial role in the cycling of bromine and ozone depletion in the region. Comparison with measured bromide in deeper snow layers will help to validate source strengths and sinks in atmospheric models. Second, the surface resistance of ozone and bromine species on different surfaces, such as ice, snow, and the ocean, needs further

revision. More consistent parameterization of these resistances is necessary to better represent these reactive species. Third, comprehensive heterogeneous and multiphase chemistry in the marine boundary layer is too computationally expensive in our current global CCM setup. Potentially, machine learning approaches could be used to bridge the gap from detailed box modeling studies to global scales. Finally, a higher model resolution could provide a more detailed representation of processes on inhomogeneous surfaces in the atmosphere-ocean-ice nexus, enhancing predictions of ozone and bromine concentrations, and contributing to a more precise understanding of their roles in the Arctic atmosphere.

470 Code availability. The Modular Earth Submodel System (MESSy) is being continuously further developed and applied by a consortium of institutions. The usage of MESSy and access to the source code is licenced to all affiliates of institutions who are members of the MESSy Consortium. Institutions can become a member of the MESSy Consortium by signing the MESSy Memorandum of Understanding. More information can be found on the MESSy Consortium website (http://www.messy-interface.org). The study presented here was performed based on MESSy version 2.55.2. Compared to MESSy v2.55.2, the updated AirSnow algorithm also includes two critical bug fixes concerning the temperature and solar zenith angle thresholds. It has been integrated into the MESSy release candidate and will be available in the next official release (version 2.56). MYSIC based on ICDC Age of Arctic Sea Ice has been contributed to the MESSy community.

Python scripts used for data processing can be made available through github.

Data availability. Data from model experiment sfa002 will be available through the Arctic Bromine Model Intercomparison project led by Jennie Thomas (IGE, Grenoble).

480 Model data from the sensitivity studies presented here can be made available upon request.

TROPOMI BrO VCD data can be made available upon request from A. Richter and B. Zilker (University of Bremen).

Surface ozone data from Alert (last access 2024-02-13), Eureka (2016–2022, last access 2025-04-15), Nord (last access 2025-04-16), Summit (last access 2024-02-12), and Zeppelin (last access 2025-04-15) used in this study were accessed from EBAS (https://ebas.nilu.no) hosted by NILU. Specifically, this includes data affiliated with the frameworks: AMAP, EMEP, GAW-WDCRG. Original data providers include: Audra McClure-Begley and Irina Petropavlovskikh (NOAA-ESRL), Wenche Aas (NILU), Mike Shaw (EC/AES), Rune Keller (NERI). Surface ozone data from Utqiagvik (Barrow, last access 2025-01-07) and Eureka (last access 2024-02-13) were provided by NOAA Global Monitoring Laboratory, Boulder, Colorado, USA (https://gml.noaa.gov).

ICDC Age of Sea Ice product is distributed by CEN, University of Hamburg.

Data used in this manuscript was produced as part of the international Multidisciplinary drifting Observatory for the Study of the Arctic 490 Climate (MOSAiC) with the tag MOSAiC20192020.

- Ozone (Angot et al., 2022)

465

485

- Bromide, bromine monoxide (Mahajan, 2022)
- Temperature, boundary layer height (Jozef et al., 2023)

The results contain modified Copernicus Climate Change Service information 2020. Neither the European Commission nor ECMWF is responsible for any use that may be made of the Copernicus information or data it contains.

Appendix A: Methods

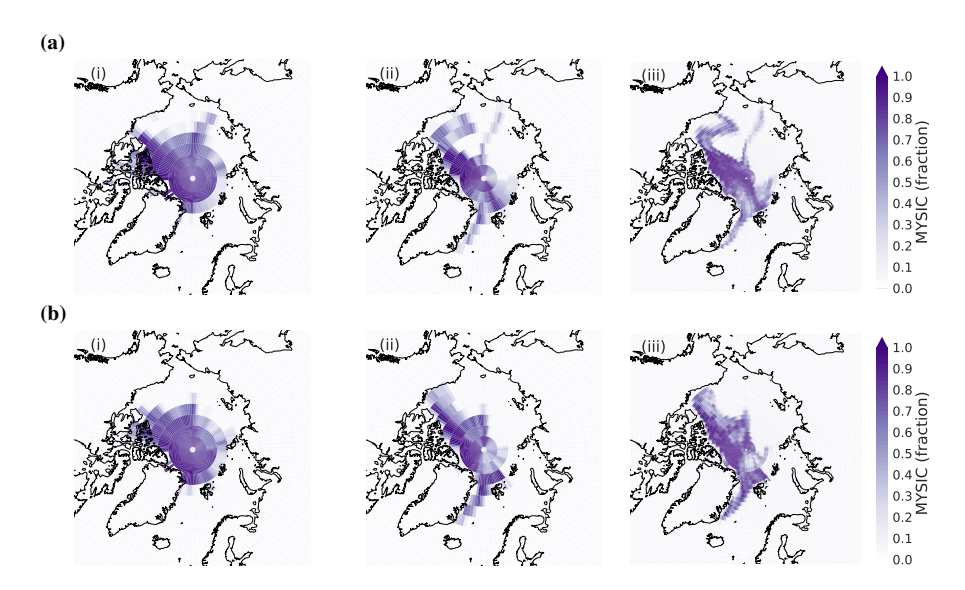


Figure A1. Maps of multi-year sea ice cover in April. (i) Estimated from ERA5 sea ice cover at seasonal low of the previous year, (ii) ICDC Age of Sea Ice product (T106). The comparison between T42 and T106 illustrates the potential benefit of a higher model resolution for resolving inhomogeneity in the characteristics of sea ice such as its age. (a) 2019; (b) 2020.

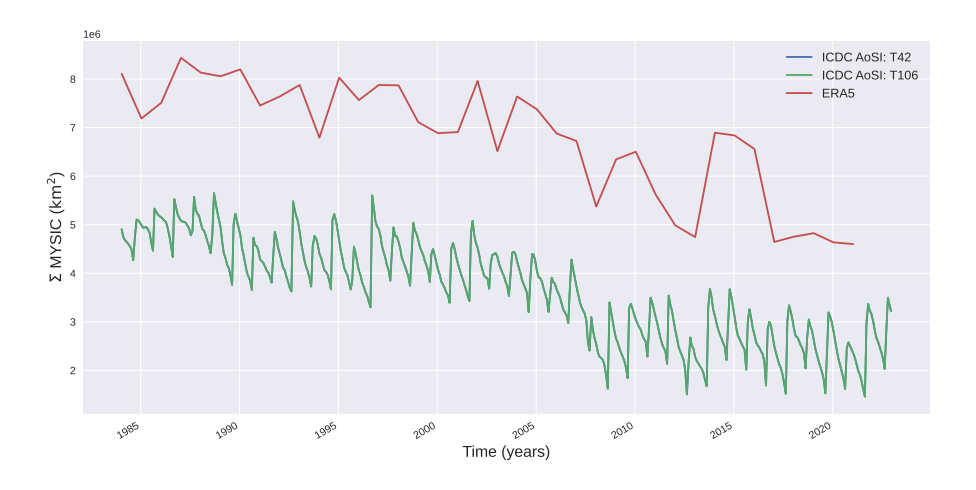


Figure A2. Annual (ERA5) and monthly (ICDC) mean time series of the total area covered by multi-year sea ice in the Arctic. MYSIC total areas estimated the two methods differ by 30%.

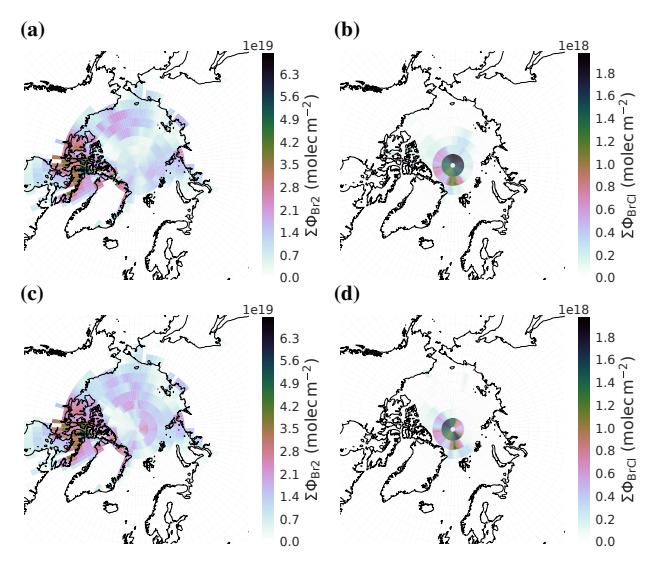


Figure A3. Comparison of modeled bromine emissions due to BEs. Flux integral of (a, c) Br₂ and (b, d) BrCl for April 2019 with MYSIC based on (a, b) ERA5 SIC (sfa008); (c, d) ICDC AoSI (sfa010).

Table A1. Model skill (R^2 and RMSE) at different Arctic ozone monitoring sites for different model experiments for spring 2019. For the respective 2d histograms and regressions see Appendix Fig. A4.

Experiment	Test	Utqiaġvik	Eureka	Summit	Zeppelin
ref	R^2	0.19	0.01	0.22	0.01
	RMSE	0.45	0.96	0.18	0.34
sfa002	\mathbb{R}^2	0.28	0.16	0.30	0.00
	RMSE	0.36	0.67	0.17	0.33
sfa008	R^2	0.29	0.17	0.29	0.00
	RMSE	0.36	0.66	0.17	0.33
sfa010	R^2	0.32	0.19	0.28	0.00
	RMSE	0.36	0.65	0.17	0.34
sfa011	\mathbb{R}^2	0.28	0.17	0.30	0.01
	RMSE	0.34	0.63	0.17	0.32
sfa012	\mathbb{R}^2	0.23	0.03	0.26	0.18
	RMSE	0.32	0.74	0.18	0.31
sfa013	\mathbb{R}^2	0.28	0.17	0.28	0.01
	RMSE	0.34	0.64	0.17	0.32
sfa017	\mathbb{R}^2	0.28	0.17	0.28	0.01
	RMSE	0.33	0.63	0.18	0.32

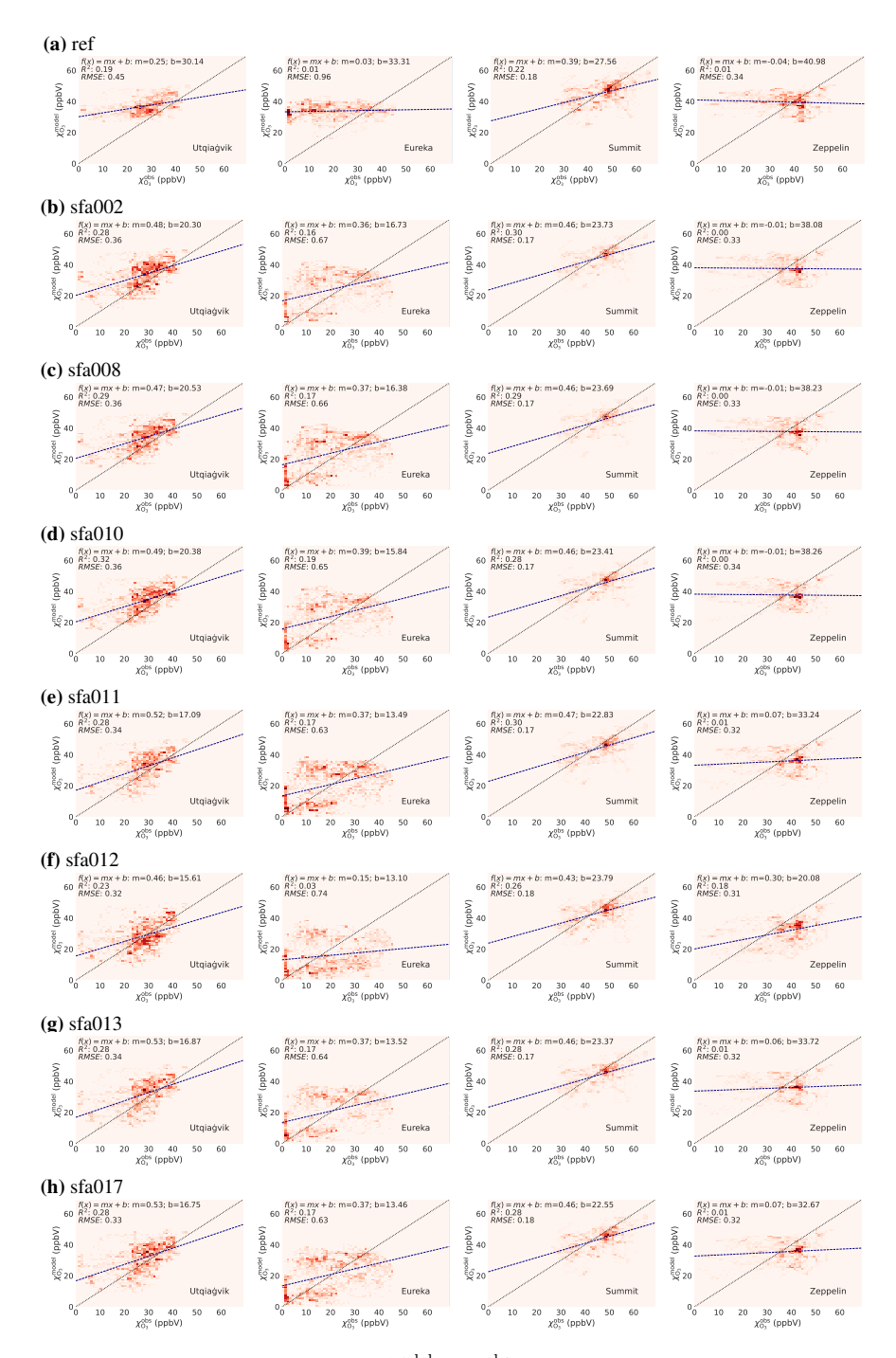


Figure A4. Sensitivity test. 2D histogram and linear fit of $\chi_{O_3}^{\text{model}}$ vs $\chi_{O_3}^{\text{obs}}$ for 2019, March–May. The respective root-mean-square error (RMSE) and coefficient of determination R^2 are listed in Appendix Table A1. From top to bottom: model experiments as given in Tab. 2. Ozone monitoring sites from left to right: Utqiaġvik, Eureka, Summit, and Zeppelin.

Appendix B: Results

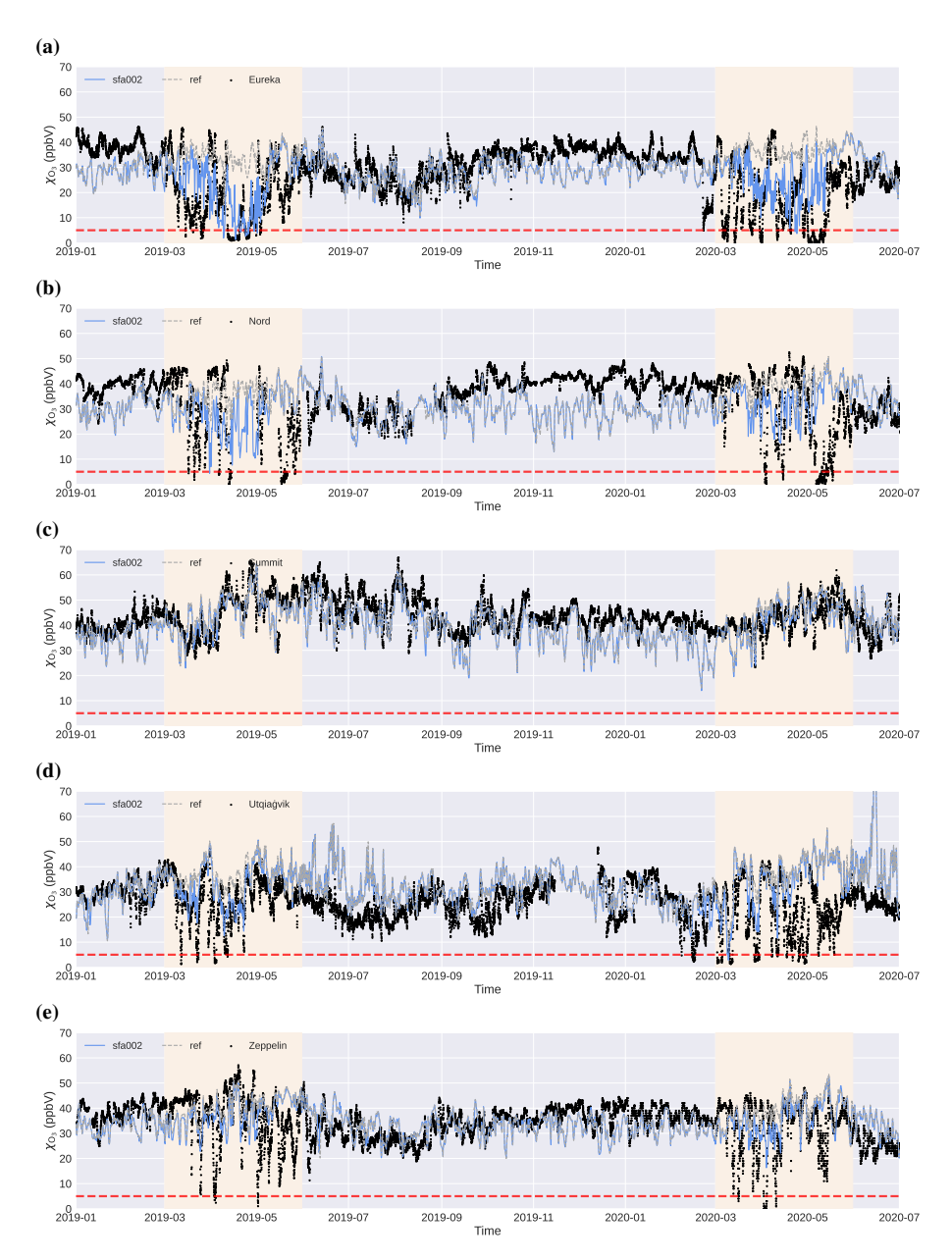


Figure B1. Time series comparing observational records of $\chi_{\rm O_3}$ at Arctic ozone monitoring sites with EMAC model output (ref, sfa002) interpolated to the station location. The periods March–May are highlighted in light yellow. The dashed red line indicates the 5 ppbv threshold for ODEs. (a) Eureka; (b) Nord; (c) Summit; (d) Utqiaġvik; (e) Zeppelin.

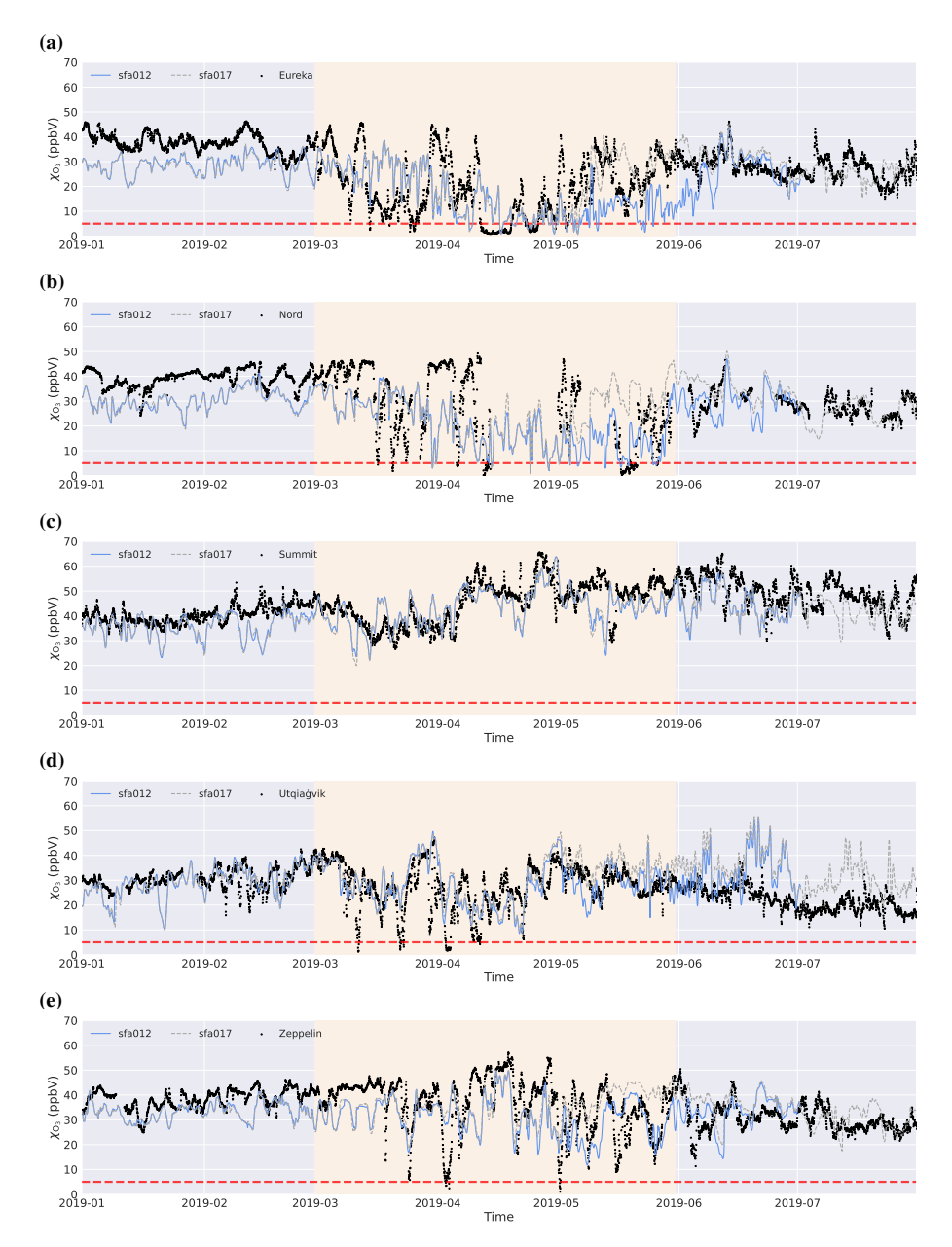


Figure B2. Time series comparing observational records of $\chi_{\rm O_3}$ at Arctic ozone monitoring sites with EMAC model output (sfa012, sefa017) interpolated to the station location. The periods March–May are highlighted in light yellow. The dashed red line indicates the 5 ppbv threshold for ODEs. (a) Eureka; (b) Nord; (c) Summit; (d) Utqiaġvik; (e) Zeppelin. For early spring (March to April), no differences are expected. The difference in $T_{\rm crit}$ will only affact May if surface temperatures rise above $-10\,^{\circ}{\rm C}$.

Table B1. Model skill (R^2 and RMSE) at different Arctic ozone monitoring sites for different model experiments in 2020.

Experiment	Test	Utqiaġvik	Eureka	Nord	Summit	Zeppelin
ref	R^2	0.06	0.03	0.09	0.17	0.00
	RMSE	0.87	1.17	0.64	0.17	0.39
sfa002	R^2	0.10	0.05	0.05	0.20	0.07
	RMSE	0.79	0.87	0.61	0.17	0.34
sfa017	R^2	0.11	0.10	0.01	0.23	0.15
	RMSE	0.71	0.74	0.62	0.16	0.30

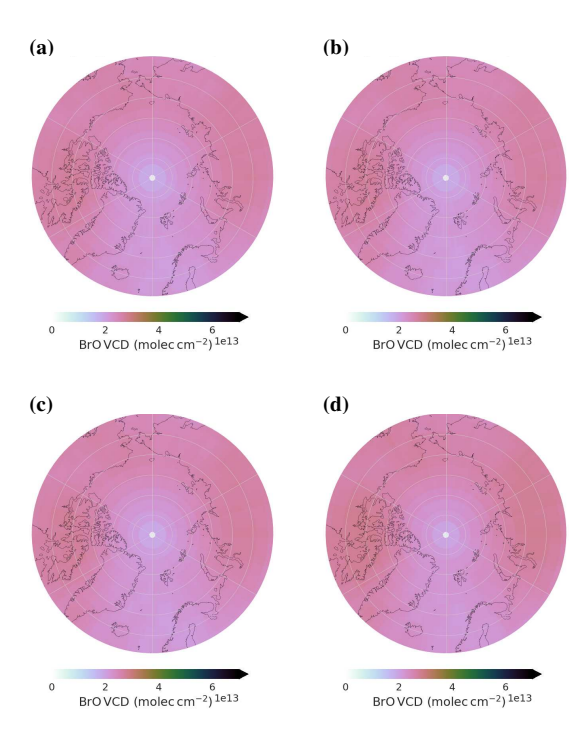


Figure B3. Monthly mean stratospheric BrO column at 13 - 14 h local time in April 2019. Shown are experiments (a) sfa008, (b) sfa010, (c) sfa013, and (d) sfa017.

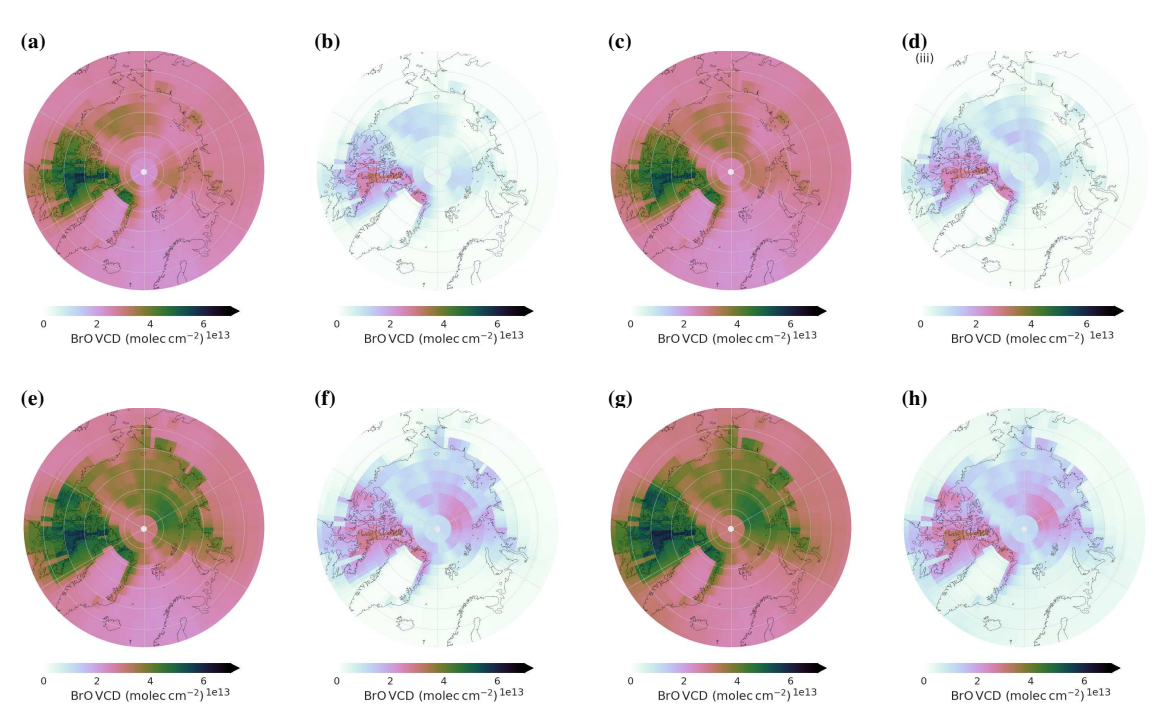


Figure B4. BrO column at 13 – 14 h local time in April 2019. (a) sfa008 (total column); (b) sfa008 (tropospheric column); (c) sfa010 (total column); (d) sfa010 (tropospheric column); (e) sfa013 (total column); (f) sfa013 (tropospheric column); (g) sfa017 (total column); (dh) sfa017 (tropospheric column). The modeled BrO total columns have been split into tropospheric and stratospheric columns using the modeled tropopause height on hourly basis.

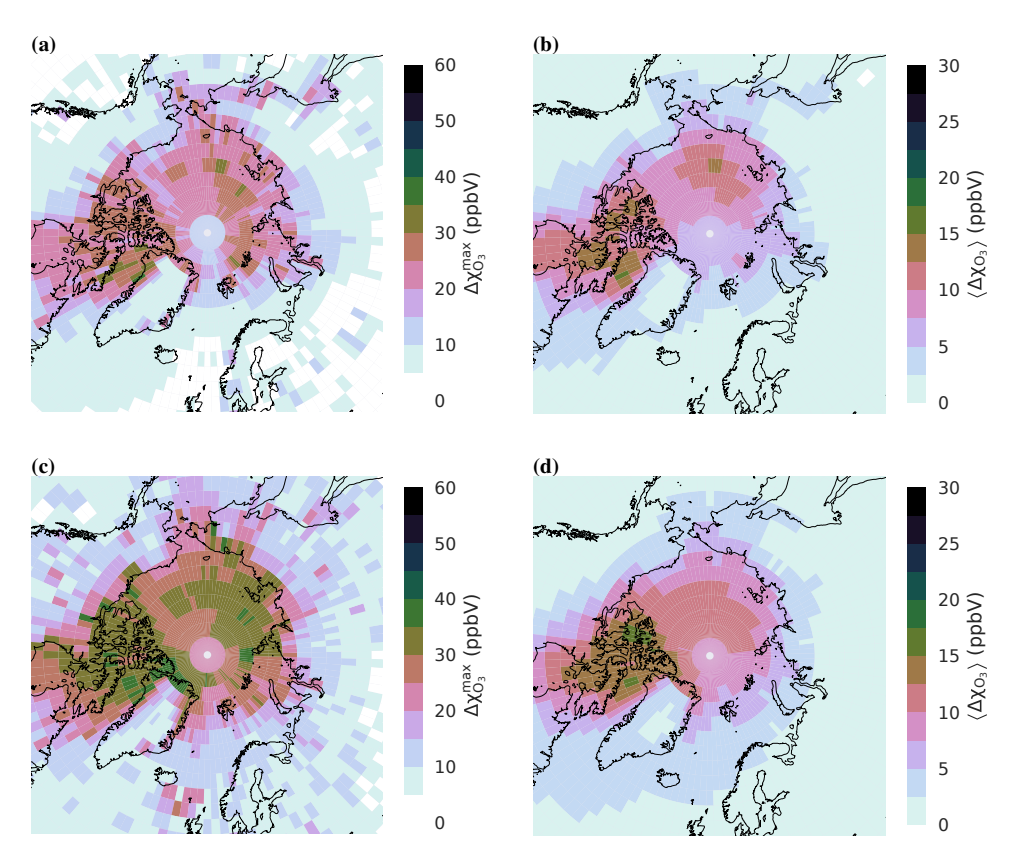


Figure B5. Monthly (a) maximum and (b) mean ozone depletion in March and (c) maximum and (d) mean ozone depletion May 2020 computed from difference between experiment sfa017 and the reference simulation.

Author contributions. SF wrote and edited the manuscript, performed the model simulations, analyzed the model results for the ozone monitoring sites, bromine fluxes, and vertical column densities, and implemented and tested the model improvements. LR contributed to the analysis of MOSAiC data including the remapping of the drift track as well as pan-Arctic ozone, improvements to the setup, and identification of model bugs. BZ performed the TROPOMI analysis. AR provided the TROPOMI data. BMS proposed the project 'BromoPole' and contributed with insights and ideas. All authors contributed to the discussion and writing of the manuscript.

Competing interests. At least one of the (co-)authors is a member of the editorial board of Atmospheric Chemistry and Physics.

500

Acknowledgements. This work was funded by the Deutsche Forschungsgemeinschaft (DFG, German Research Foundation) '517648310'.

This work was performed on the HoreKa supercomputer funded by the Ministry of Science, Research and the Arts Baden-Württemberg. The authors would like to thank the German Federal Ministry of Education and Research and the German federal states (http://www.nhr-verein.de/en/our-partners) for supporting this work as part of the National High-Performance Computing (NHR) joint funding program. We gratefully acknowledge the funding by the DFG – project no. 268020496 - TRR 172, within the Transregional Collaborative Research Center "ArctiC Amplification: Climate relevant Atmospheric and SurfaCe Processes, and Feedback Mechanisms (AC)3".

The authors like to thank Patrick Jöckel (DLR) for his helpful comments and insights regarding the MESSy framework and submodel setup. Special thanks go to Ole Kirner (SimLab, KIT) and Sören Johansson (IMKASF) for valuable help for the model and machine setup. Thanks to ICDC, CEN, University of Hamburg for data support, especially Stefan Kern. We thank all those who contributed to MOSAiC and made this endeavour possible (Nixdorf et al., 2021).

We thank Jennie Thomas (CNRS, Institut des Géosciences de l'Environnement, Grenoble, France) for organizing the Arctic Bromine

Model Intercomparison project, which is a part of CATCH (the Cryosphere and Atmospheric Chemistry) and to which we contributed with parts of this work.

ChatGPT has been utilized to generate the manuscript abstract and title based on the Section "discussions and conclusions" as well as word smithing the outlook summary from a list of key points.

References

- Abbatt, T. P. D., Thomas, J. L., Abrahamsson, K., Boxxe, C., Granfors, A., Jones, A. E., King, M. D., Saiz-Lopez, A., Shepson, P. B., Sodeau, J., Toohey, D. W.and Toubin, C., von Glasow, R., Wren, S. N., and Yang, X.: Halogene activation via interactions with environmental ice and snow in the polar lower troposphere and other regions, Atmos. Chem. Phys., 12, 6237–6271, https://doi.org/10.5194/acp-12-6237-2012, 2012.
- Abrahamsson, K., Granfors, A., Ahnoff, M., Cuevas, C. A., and Saiz-Lopez, A.: Organic bromine compounds produced in sea ice in Antarctic winter, Nature Communications, 9, https://doi.org/10.1038/s41467-018-07062-8, 2018.
 - Ackermann, I. J., Hass, H., Memmesheimer, M., Ebel, A., Binkowski, F. S., and Shankar, U.: Modal aerosol dynamics model for Europe: development and first applications, Atmospheric Environment, 32, 2981–2999, https://doi.org/10.1016/S1352-2310(98)00006-5, 1998.
 - Adams, J. W., Holmes, N. S., and Crowley, J. N.: Uptake and reaction of HOBr on frozen and dry NaCl/NaBr surfaces between 253 and 233 K, Atmos. Chem. Phys., 2, 79–91, https://doi.org/10.5194/acp-2-79-2002, 2002.
- AMAP: Arctic Climate Issues 2011: Changes in Arctic Snow, Water, Ice and Permafrost, Overview Report, SWIPA 2011, Arctic Monitoring and Assessment Programme (AMAP), Oslo, 978-82-7971-073-8, 2012.
 - Angot, H., Blomquist, B., Howard, D., Archer, S., Bariteau, L., Beck, I., Helmig, D., Hueber, J., Jacobi, H.-W., Jokinen, T., Laurila, T., Posman, K., Quéléver, L., Shupe, M. D., Schmale, J., and Boyer, M.: Ozone dry air mole fractions measured during MOSAiC 2019/2020 (merged dataset), https://doi.org/10.1594/PANGAEA.944393, 2022.
- Baker, K., Woody, M., Tonnesen, G., Hutzell, W., Pye, H., Beaver, M., Pouliot, G., and Pierce, T.: Contribution of regional-scale fire events to ozone and PM2.5 air quality estimated by photochemical modeling approaches, Atmos. Environ., 140, 539–554, https://doi.org/10.1016/j.atmosenv.2016.06.032, 2016.
 - Barrie, L. A., Bottenheim, J. W., Schnell, R. C., Crutzen, P. J., and Rasmussen, R. A.: Ozone destruction and photochemical reactions at polar sunrise in the lower Arctic atmosphere, Nature, 334, 138–141, https://doi.org/10.1038/334138a0, 1988.
- Barten, J. G., Ganzeveld, L. N., Steeneveld, G.-J., Blomquist, B. W., Angot, H., Archer, S. D., Bariteau, L., Beck, I., Boyer, M., von der Gathen, P., Helmig, D., Howard, D., Hueber, J., Jacobi, H.-W., Jokinen, T., Laurila, T., Posman, K. M., Quéléver, L., Schmale, J., Shupe, M. D., and Krol, M. C.: Low ozone dry deposition rates to sea ice during the MOSAiC field campaign: Implications for the Arctic boundary layer ozone budget, Elementa-Sci. Anthrop., 11, 00 086, https://doi.org/10.1525/elementa.2022.00086, 2023.
- Benavent, N., Mahajan, A. S., Li, Q., Cuevas, C. A., Schmale, J., Angot, H., Jokinen, T., Quéléver, L. L. J., Blechschmidt, A.-M., Zilker,
 B., Richter, A., Serna, J. A., Garcia-Nieto, D., Fernandez, R. P., Skov, H., Dumitrascu, A., Simões Pereira, P., Abrahamsson, K., Bucci,
 S., Duetsch, M., Stohl, A., Beck, I., Laurila, T., Blomquist, B., Howard, D., Archer, S. D., Bariteau, L., Helmig, D., Hueber, J., Jacobi,
 H.-W., Posman, K., Dada, L., Daellenbach, K. R., and Saiz-Lopez, A.: Substantial contribution of iodine to Arctic ozone destruction, Nat.
 Geosci., 15, 770–773, https://doi.org/10.1038/s41561-022-01018-w, 2022.
- Bottenheim, J. W., Gallant, A. G., and Brice, K. A.: Measurements of NOy Species and O-3 at 82-Degrees-N Latitude, Geophys. Res. Lett., 13, 113–116, https://doi.org/10.1029/GL013i002p00113, 1986.
 - Bougoudis, I., Blechschmidt, A.-M., Richter, A., Seo, S., Burrows, J. P., Theys, N., and Rinke, A.: Long-term time series of Arctic tropospheric BrO derived from UV–VIS satellite remote sensing and its relation to first-year sea ice, Atmos. Chem. Phys., 20, 11869–11892, https://doi.org/10.5194/acp-20-11869-2020, 2020.

- Bozem, H., Hoor, P., Kunkel, D., Köllner, F., Schneider, J., Herber, A., Schulz, H., Leaitch, W. R., Aliabadi, A. A., Willis, M. D., Burkart,

 J., and Abbatt, J. P. D.: Characterization of transport regimes and the polar dome during Arctic spring and summer using in situ aircraft measurements, Atmos. Chem. Phys., 19, 15 049–15 071, https://doi.org/10.5194/acp-19-15049-2019, 2019.
 - Brooks, S. B., Saiz-Lopez, A., Skov, H., Lindberg, S. E., Plane, J. M. C., and Goodsite, M. E.: The mass balance of mercury in the springtime arctic environment, Geophys. Res. Lett., 33, 1–4, https://doi.org/10.1029/2005GL025525, 2006.
- Burd, J. A., Peterson, P. K., Nghiem, S. V., Perovich, D. K., and Simpson, W. R.: Snowmelt onset hinders bromine monoxide heterogeneous recycling in the Arctic, J. Geophys. Res. Atmos., 122, 8297–8309, https://doi.org/10.1002/2017JD026906, 2017.
 - Carns, R. C., Brandt, R. E., and Warren, S. G.: Salt precipitation in sea ice and its effect on albedo, with application to Snowball Earth, J. Geophys. Res. Oceans, 120, 7400–7412, https://doi.org/10.1002/2015JC011119, 2015.
 - Choi, S., Wang, Y., Salawitch, R. J., Canty, T., Joiner, J., Zeng, T., Kurosu, T. P., Chance, K., Richter, A., Huey, L. G., Liao, J., Neuman, J. A., Nowak, J. B., Dibb, J. E., Weinheimer, A. J., Diskin, G., Ryerson, T. B., da Silva, A., Curry, J., Kinnison, D., Tilmes, S., and Levelt, P. F.:
- Analysis of satellite-derived Arctic tropospheric BrO columns in conjunction with aircraft measurements during ARCTAS and ARCPAC, Atmos. Chem. Phys., 12, 1255–1285, https://doi.org/10.5194/acp-12-1255-2012, 2012.
 - Cofer, W. R., Levine, J. S., Winstead, E. L., and Stocks, B. J.: Gaseous emissions from Canadian boreal forest fires, Atmos. Environ., 24, 1653–1659, https://doi.org/10.1016/0960-1686(90)90499-D, 1990.
- Descals, A., Gaveau, D. L. A., Verger, A., Sheil, D., Naito, D., and Peñuelas, J.: Unprecedented fire activity above the Arctic Circle linked to rising temperatures, Sci., 378, 532–537, https://doi.org/10.1126/science.abn9768, 2022.
 - Edebeli, J., Trachsel, J. C., Avak, S. E., Ammann, M., Schneebeli, M., Eichler, A., and Bartels-Rausch, T.: Snow heterogeneous reactivity of bromide with ozone lost during snow metamorphism, Atmos. Chem. Phys., 20, 13 443–13 454, https://doi.org/10.5194/acp-20-13443-2020, 2020.
- Falk, S. and Sinnhuber, B.-M.: Polar boundary layer bromine explosion and ozone depletion events in the chemistry-climate model EMAC v2.52: implementation and evaluation of AirSnow algorithm, Geosci. Model Dev., 11, 1115–1131, https://doi.org/10.5194/gmd-11-1115-2018, 2018.
 - Fernandez, R. P., Berná, L., Tomazzeli, O. G., Mahajan, A. S., Li, Q., Kinnison, D. E., Wang, S., Lamarque, J.-F., Tilmes, S., Skov, H., Cuevas, C. A., and Saiz-Lopez, A.: Arctic halogens reduce ozone in the northern mid-latitudes, Proc. Natl. Acad. Sci., 121, 9, https://doi.org/10.1073/pnas.2401975121, 2024.
- Fickert, S., Adams, J. W., and Crowley, J. N.: Activation of Br2 and BrCl via uptake of HOBr onto aqueous salt solutions, J. Geophys. Res. Atmos., 104, 23719–23727, https://doi.org/10.1029/1999JD900359, 1999.

- Gong, W., Beagley, S. R., Toyota, K., Skov, H., Christensen, J. H., Lupu, A., Pendlebury, D., Zhang, J., Im, U., Kanaya, Y., Saiz-Lopez, A., Sommariva, R., Effertz, P., Halfacre, J. W., Jepsen, N., Kivi, R., Koenig, T. K., Müller, K., Nordstrøm, C., Petropavlovskikh, I., Shepson, P. B., Simpson, W. R., Solberg, S., Staebler, R. M., Tarasick, D. W., Van Malderen, R., and Vestenius, M.: Modelling Arctic lower-tropospheric ozone: processes controlling seasonal variations, Atmos. Chem. Phys., 25, 8355–8405, https://doi.org/10.5194/acp-25-8355-2025, 2025.
- Guelle, W., Schulz, M., Balkanski, Y., and Dentener, F.: Influence of the source formulation on modeling the atmospheric global distribution of sea salt aerosol, J. Geophys. Res. Atmos., 106, 27 509–27 524, https://doi.org/10.1029/2001JD900249, 2001.
- Haine, T. W. N. and Martin, T.: The Arctic-Subarctic sea ice system is entering a seasonal regime: Implications for future Arctic amplification, Sci. Rep., 7, 2045–2322, https://doi.org/10.1038/s41598-017-04573-0, 2017.

- Hausmann, M. and Platt, U.: Spectroscopic measurement of bromine oxide and ozone in the high Arctic during Polar Sunrise Experiment 1992, J. Geophys. Res. Atmos., 99, 25 399–25 413, https://doi.org/10.1029/94JD01314, 1994.
- Helmig, D., Oltmans, S. J., Carlson, D., Lamarque, J.-F., Jones, A., Labuschagne, C., Anlauf, K., and Hayden, K.: A review of surface ozone in the polar regions, Atmos. Environ., 41, 5138–5161, https://doi.org/10.1016/j.atmosenv.2006.09.053, recent Investigations of Snow Photochemistry and Air-Snow Exchange at Summit, Greenland, 2007.

- Hersbach, H., Bell, B., Berrisford, P., Hirahara, S., Horányi, A., Muñoz-Sabater, J., Nicolas, J., Peubey, C., Radu, R., Schepers, D., Simmons, A., Soci, C., Abdalla, S., Abellan, X., Balsamo, G., Bechtold, P., Biavati, G., Bidlot, J., Bonavita, M., De Chiara, G., Dahlgren, P., Dee, D., Diamantakis, M., Dragani, R., Flemming, J., Forbes, R., Fuentes, M., Geer, A., Haimberger, L., Healy, S., Hogan, R. J., Hólm, E., Janisková, M., Keeley, S., Laloyaux, P., Lopez, P., Lupu, C., Radnoti, G., de Rosnay, P., Rozum, I., Vamborg, F., Villaume, S., and Thépaut, J.-N.: The ERA5 global reanalysis, O. J. R. Meteorol, Soc., 146, 1999–2049, https://doi.org/10.1002/qi.3803, 2020.
- Jacobi, H. W., Morin, S., and Bottenheim, J. W.: Observation of widespread depletion of ozone in the springtime boundary layer of the central Arctic linked to mesoscale synoptic conditions, J. Geophys. Res. Atmos., 115, https://doi.org/10.1029/2010JD013940, 2010.
- Jones, A. E., Wolff, E. W., Salmon, R. A., Bauguitte, S. J.-B., Roscoe, H. K., Anderson, P. S., Ames, D., Clemitshaw, K. C., Fleming, Z. L., Bloss, W. J., Heard, D. E., Lee, J. D., Read, K. A., Hamer, P., Shallcross, D. E., Jackson, A. V., Walker, S. L., Lewis, A. C., Mills, G. P.,
- Plane, J. M. C., Saiz-Lopez, A., Sturges, W. T., and Worton, D. R.: Chemistry of the Antarctic Boundary Layer and the Interface with Snow: an overview of the CHABLIS campaign, Atmos. Chem. Phys., 8, 3789–3803, https://doi.org/10.5194/acp-8-3789-2008, 2008.
 - Jones, A. E., Anderson, P. S., Begoin, M., Brough, N., Hutterli, M. A., Marshall, G. J., Richter, A., Roscoe, H. K., and Wolff, E. W.: BrO, blizzards, and drivers of polar tropospheric ozone depletion events, Atmos. Chem. Phys., 9, 4639–4652, https://doi.org/10.5194/acp-9-4639-2009, 2009.
- 610 Jozef, G., Klingel, R., Cassano, J. J., Maronga, B., de Boer, G., Dahlke, S., and Cox, C. J.: Lower atmospheric properties relating to temperature, wind, stability, moisture, and surface radiation budget over the central Arctic sea ice during MOSAiC, https://doi.org/10.1594/PANGAEA.957760, 2023.
 - Jöckel, P., Sander, R., Kerkweg, A., Tost, H., and Lelieveld, J.: Technical Note: The Modular Earth Submodel System (MESSy) a new approach towards Earth System Modeling, Atmos. Chem. Phys., 5, 433–444, https://doi.org/10.5194/acp-5-433-2005, 2005.
- Jöckel, P., Tost, H., Pozzer, A., Kunze, M., Kirner, O., Brenninkmeijer, C. A. M., Brinkop, S., Cai, D. S., Dyroff, C., Eckstein, J., Frank, F., Garny, H., Gottschaldt, K.-D., Graf, P., Grewe, V., Kerkweg, A., Kern, B., Matthes, S., Mertens, M., Meul, S., Neumaier, M., Nuetzel, M., Oberlaender-Hayn, S., Ruhnke, R., Runde, T., Sander, R., Scharffe, D., and Zahn, A.: Earth System Chemistry integrated Modelling (ES-CiMo) with the Modular Earth Submodel System (MESSy) version 2.51, Geosci. Model Dev., 9, 1153–1200, https://doi.org/10.5194/gmd-9-1153-2016, 2016.
- Karlsson, P., Ferm, M., Tømmervik, H., Hole, L., Karlsson, G., Ruoho-Airola, T., Aas, W., Hellsten, S., Akselsson, C., Mikkelsen, T., and Nihlgård, B.: Biomass burning in eastern Europe during spring 2006 caused high deposition of ammonium in northern Fennoscandia, Environ. Pollut., 176C, 71–79, https://doi.org/10.1016/j.envpol.2012.12.006, 2013.
 - Kerkweg, A.: Global Modelling of Atmospheric Halogen Chemistry in the Marine Boundary Layer, Ph.D. thesis, Rheinische Friedrich-Wilhelms-Universität Bonn, https://nbn-resolving.org/urn:nbn:de:hbz:5N-06365, 2005.
- Kerkweg, A., Buchholz, J., Ganzeveld, L., Pozzer, A., Tost, H., and Jöckel, P.: Technical Note: An implementation of the dry removal processes DRY DEPosition and SEDImentation in the Modular Earth Submodel System (MESSy), Atmos. Chem. Phys., 6, 4617–4632, https://doi.org/10.5194/acp-6-4617-2006, 2006a.

- Kerkweg, A., Sander, R., Tost, H., and Jöckel, P.: Technical note: Implementation of prescribed (OFFLEM), calculated (ONLEM), and pseudo-emissions (TNUDGE) of chemical species in the Modular Earth Submodel System (MESSy), Atmos. Chem. Phys., 6, 3603–3609, https://doi.org/10.5194/acp-6-3603-2006, 2006b.
 - Koop, T., Kapilashrami, A., Molina, L. T., and Molina, M. J.: Phase transitions of sea-salt/water mixtures at low temperatures: Implications for ozone chemistry in the polar marine boundary layer, J. Geophys. Res. Atmos., 105, 26 393–26 402, https://doi.org/10.1029/2000JD900413, 2000.
- Lary, D. and McQuaid, J.: Diffuse radiation, twilight, and photochemistry ? II, J. Atmos. Chem., 13, 373–392, 635 https://doi.org/10.1007/BF00057753, 1991.
 - Lindsay, R. and Schweiger, A.: Arctic sea ice thickness loss determined using subsurface, aircraft, and satellite observations, The Cryosphere, 9, 269–283, https://doi.org/10.5194/tc-9-269-2015, 2015.
 - Lindskog, A., Karlsson, P., Grennfelt, P., Solberg, S., and Forster, C.: An exceptional ozone episode in northern Fennoscandia, Atmos. Environ., 41, 950–958, https://doi.org/10.1016/j.atmosenv.2006.09.027, 2007.
- Luhar, A. K., Woodhouse, M. T., and Galbally, I. E.: A revised global ozone dry deposition estimate based on a new two-layer parameterisation for air-sea exchange and the multi-year MACC composition reanalysis, Atmos. Chem. Phys., 18, 4329–4348, https://doi.org/10.5194/acp-18-4329-2018, 2018.
 - Mahajan, A.: Substantial contribution of iodine to Arctic ozone destruction data, https://doi.org/10.17632/BN7YTZ4MFZ.1, 2022.
- Marelle, L., Thomas, J. L., Ahmed, S., Tuite, K., Stutz, J., Dommergue, A., Simpson, W. R., Frey, M. M., and Baladima, F.: Implementation and Impacts of Surface and Blowing Snow Sources of Arctic Bromine Activation Within WRF-Chem 4.1.1, J. Adv. Model. Earth Syst., 13, https://doi.org/10.1029/2020MS002391, 2021.
 - McClure-Begley, A., Petropavlovskikh, I., and Oltmans, S.: Barrow Atmospheric Baseline Observatory, 1973–2023-10, https://doi.org/http://dx.doi.org/10.7289/V57P8WBF, last accessed July 2024, 2024.
 - McConnell, J. C., Henderson, G. S., Barrie, L., Bottenheim, J., Niki, H., Langford, C. H., and Tempelton, E. M. J.: Photochemical Bromine Production Implicated in Arctic Boundary-Layer Ozone Depletion, Nature, 355, 150–152, https://doi.org/10.1038/355150a0, 1992.

- Nixdorf, U., Dethloff, K., Rex, M., Shupe, M., Sommerfeld, A., Perovich, D. K., Nicolaus, M., Heuzé, C., Rabe, B., Loose, B., Damm, E., Gradinger, R., Fong, A., Maslowski, W., Rinke, A., Kwok, R., Spreen, G., Wendisch, M., Herber, A., Hirsekorn, M., Mohaupt, V., Frickenhaus, S., Immerz, A., Weiss-Tuider, K., König, B., Mengedoht, D., Regnery, J., Gerchow, P., Ransby, D., Krumpen, T., Morgenstern, A., Haas, C., Kanzow, T., Rack, F. R., Saitzev, V., Sokolov, V., Makarov, A., Schwarze, S., Wunderlich, T., Wurr, K., and Boetius, A.: MOSAiC Extended Acknowledgement, https://doi.org/10.5281/ZENODO.5541624, 2021.
- Norsk institutt for luftforskning (NILU): Database for observation data of atmospheric chemical composition and physical properties, online, http://ebas.nilu.no/, last accessed July 2024.
- Notz, D. and SIMIP Community: Arctic Sea Ice in CMIP6, Geophys. Res. Lett., 47, e2019GL086749, https://doi.org/10.1029/2019GL086749, 2020.
- Oldridge, N. W. and Abbatt, J. P. D.: Formation of Gas-Phase Bromine from Interaction of Ozone with Frozen and Liquid Na-Cl/NaBr Solutions: Quantitative Separation of Surficial Chemistry from Bulk-Phase Reaction, J. Phys. Chem. A, 115, 2590–2598, https://doi.org/10.1021/jp200074u, 2011.
- Orbe, C., Plummer, D. A., Waugh, D. W., Yang, H., Jöckel, P., Kinnison, D. E., Josse, B., Marecal, V., Deushi, M., Abraham, N. L., Archibald, A. T., Chipperfield, M. P., Dhomse, S., Feng, W., and Bekki, S.: Description and Evaluation of the specified-dynamics experiment in the Chemistry-Climate Model Initiative, Atmos. Chem. Phys., 20, 3809–3840, https://doi.org/10.5194/acp-20-3809-2020, 2020.

- Peterson, P. K., Hartwig, M., May, N. W., Schwartz, E., Rigor, I., Ermold, W., Steele, M., Morison, J. H., Nghiem, S. V., and Pratt, K. A.: Snowpack measurements suggest role for multi-year sea ice regions in Arctic atmospheric bromine and chlorine chemistry, Elementa-Sci Anthrop., 7, 14, https://doi.org/10.1525/elementa.352, 2019.
- Platt, U. and Hönninger, G.: The role of halogen species in the troposphere, Chemosphere, 52, 325–338, https://doi.org/10.1016/S0045-6535(03)00216-9, naturally Produced Organohalogens, 2003.
 - Pound, R. J., Sherwen, T., Helmig, D., Carpenter, L. J., and Evans, M. J.: Influences of oceanic ozone deposition on tropospheric photochemistry, Atmos. Chem. Phys., 20, 4227–4239, https://doi.org/10.5194/acp-20-4227-2020, 2020.
 - Pozzer, A., Jöckel, P., Sander, R., Williams, J., Ganzeveld, L., and Lelieveld, J.: Technical Note: The MESSy-submodel AIRSEA calculating the air-sea exchange of chemical species, Atmospheric Chemistry and Physics, 6, 5435–5444, https://doi.org/10.5194/acp-6-5435-2006, 2006.

- Rantanen, M., Karpechko, A., Lipponen, A., Nordling, K., Hyvärinen, O., Ruosteenoja, K., Vihma, T., and Laaksonen, A.: The Arctic has warmed nearly four times faster than the globe since 1979, Commun. Earth Environ., pp. 1–10, https://doi.org/10.1038/s43247-022-00498-3, 2022.
- Regan, H., Rampal, P., Ólason, E., Boutin, G., and Korosov, A.: Modelling the evolution of Arctic multiyear sea ice over 2000–2018, The Cryosphere, 17, 1873–1893, https://doi.org/10.5194/tc-17-1873-2023, 2023.
 - Richter, A., Wittrock, F., Ladstätter-Weißenmayer, A., and Burrows, J.: Gome measurements of stratospheric and tropospheric BrO, Adv. Space. Res., 29, 1667–1672, https://doi.org/10.1016/S0273-1177(02)00123-0, 2002.
 - Richter, A., Wittrock, F., Eisinger, M., and Burrows, J. P.: GOME observations of tropospheric BrO in northern hemispheric spring and summer 1997, Geophys. Res. Lett., 25, 2683–2686, https://doi.org/10.1029/98GL52016, 1998.
- Ridley, B. A., Atlas, E. L., Montzka, D. D., Browell, E. V., Cantrell, C. A., Blake, D. R., Blake, N. J., Cinquini, L., Coffey, M. T., Emmons, L. K., Cohen, R. C., DeYoung, R. J., Dibb, J. E., Eisele, F. L., Flocke, F. M., Fried, A., Grahek, F. E., Grant, W. B., Hair, J. W., Hannigan, J. W., Heikes, B. J., Lefer, B. L., Mauldin, R. L., Moody, J. L., Shetter, R. E., Snow, J. A., Talbot, R. W., Thornton, J. A., Walega, J. G., Weinheimer, A. J., Wert, B. P., and Wimmers, A. J.: Ozone depletion events observed in the high latitude surface layer during the TOPSE aircraft program, J. Geophys. Res. Atmos., 108, 1–22, https://doi.org/10.1029/2001JD001507, 2003.
- Salawitch, R. J., Canty, T., Kurosu, T., Chance, K., Liang, Q., da Silva, A., Pawson, S., Nielsen, J. E., Rodriguez, J. M., Bhartia, P. K., Liu, X., Huey, L. G., Liao, J., Stickel, R. E., Tanner, D. J., Dibb, J. E., Simpson, W. R., Donohoue, D., Weinheimer, A., Flocke, F., Knapp, D., Montzka, D., Neuman, J. A., Nowak, J. B., Ryerson, T. B., Oltmans, S., Blake, D. R., Atlas, E. L., Kinnison, D. E., Tilmes, S., Pan, L. L., Hendrick, F., Van Roozendael, M., Kreher, K., Johnston, P. V., Gao, R. S., Johnson, B., Bui, T. P., Chen, G., Pierce, R. B., Crawford, J. H., and Jacob, D. J.: A new interpretation of total column BrO during Arctic spring, Geophys. Res. Lett., 37, 9, https://doi.org/10.1029/2010GL043798, 2010.
 - Sander, R., Burrows, J., and Kaleschke, L.: Carbonate precipitation in brine a potential trigger for tropospheric ozone depletion events, Atmos. Chem. Phys., 6, 4653–4658, https://doi.org/10.5194/acp-6-4653-2006, 2006.
 - Sander, R., Baumgaertner, A., Cabrera-Perez, D., Frank, F., Gromov, S., Grooß, J. U., Harder, H., Huijnen, V., Jöckel, P., Karydis, V. A., Niemeyer, K. E., Pozzer, A., Riede, H., Schultz, M. G., Taraborrelli, D., and Tauer, S.: The community atmospheric chemistry box model CAABA/MECCA-4.0, Geosci. Model Dev., 12, 1365–1385, https://doi.org/10.5194/gmd-12-1365-2019, 2019.
 - Seo, S., Richter, A., Blechschmidt, A. M., Bougoudis, I., and Burrows, J. P.: First high-resolution BrO column retrievals from TROPOMI, Atmos. Meas. Tech., 12, 2913–2932, https://doi.org/10.5194/amt-12-2913-2019, 2019.

- Seo, S., Richter, A., Blechschmidt, A. M., Bougoudis, I., and Burrows, J. P.: Spatial distribution of enhanced BrO and its relation to meteorological parameters in Arctic and Antarctic sea ice regions, Atmos. Chem. Phys., 20, 12285–12312, https://doi.org/10.5194/acp-20-12285-2020, 2020.
 - Steinbrecht, W., Kubistin, D., Plass-Dülmer, C., Davies, J., Tarasick, D. W., von der Gathen, P., Deckelmann, H., Jepsen, N., Kivi, R., Lyall, N., Palm, M., Notholt, J., Kois, B., Oelsner, P., Allaart, M., Piters, A., Gill, M., Van Malderen, R., Delcloo, A. W., Sussmann, R., Mahieu, E., Servais, C., Romanens, G., Stübi, R., Ancellet, G., Godin-Beekmann, S., Yamanouchi, S., Strong, K., Johnson, B., Cullis, P., Petropavlovskikh, I., Hannigan, J. W., Hernandez, J.-L., Diaz Rodriguez, A., Nakano, T., Chouza, F., Leblanc, T., Torres, C., Garcia, O.,
- Röhling, A. N., Schneider, M., Blumenstock, T., Tully, M., Paton-Walsh, C., Jones, N., Querel, R., Strahan, S., Stauffer, R. M., Thompson, A. M., Inness, A., Engelen, R., Chang, K.-L., and Cooper, O. R.: COVID-19 Crisis Reduces Free Tropospheric Ozone Across the Northern Hemisphere, Geophys. Res. Lett., 48, 11, https://doi.org/10.1029/2020GL091987, 2021.
 - Stemmler, I., Hense, I., and Quack, B.: Marine sources of bromoform in the global open ocean global patterns and emissions, Biogeosciences, 12, 1967–1981, https://doi.org/10.5194/bg-12-1967-2015, 2015.
- 715 Stroeve, J. and Notz, D.: Changing state of Arctic sea ice across all seasons, Environ. Res. Lett., 13, 1–23, https://doi.org/10.1088/1748-9326/aade56, 2018.

725

https://doi.org/10.5194/acp-11-3949-2011, 2011.

- Theys, N., Van Roozendael, M., Errera, Q., Hendrick, F., Daerden, F., Chabrillat, S., Dorf, M., Pfeilsticker, K., Rozanov, A., Lotz, W., Burrows, J., Lambert, J., Goutail, F., Roscoe, H., and Demazì Ere, M.: Atmos. Chem. Phys. A global stratospheric bromine monoxide climatology based on the BASCOE chemical transport model, Atmos. Chem. Phys, 9, 831–848, https://doi.org/10.5194/acp-9-831-2009, 2009.
- Tost, H., Jöckel, P. J., Kerkweg, A., Sander, R., and Lelieveld, J.: Technical note: A new comprehensive SCAVenging submodel for global atmospheric chemistry modelling, Atmos. Chem. Phys., 6, 565–574, 2006.
- Toyota, K., McConnell, J. C., Lupu, A., Neary, L., McLinden, C. A., Richter, A., Kwok, R., Semeniuk, K., Kaminski, J. W., Gong, S. L., Jarosz, J., Chipperfield, M. P., and Sioris, C. E.: Analysis of reactive bromine production and ozone depletion in the Arctic boundary layer using 3-D simulations with GEM-AQ: inference from synoptic-scale patterns, Atmos. Chem. Phys., 11, 3949–3979,
- Toyota, K., McConnell, J. C., Staebler, R. M., and Dastoor, A. P.: Air-snowpack exchange of bromine, ozone and mercury in the springtime Arctic simulated by the 1-D model PHANTAS Part 1: In-snow bromine activation and its impact on ozone, Atmos. Chem. Phys., 14, 4101–4133, https://doi.org/10.5194/acp-14-4101-2014, 2014.
- Tschudi, M., Meier, W. N., Stewart, J. S., Fowler, C., and Maslanik, J.: EASE-Grid Sea Ice Age, Version 4.1, [northern hemisphere, 1983–2023], Tech. rep., NASA National Snow and Ice Data Center Distributed Active Archive Center, Boulder, Colorado USA, https://doi.org/10.5067/UTAV7490FEPB, last accessed August 2023, 2024.
 - Venter, Z. S., Aunan, K., Chowdhury, S., and Lelieveld, J.: COVID-19 lockdowns cause global air pollution declines, Proc. Natl. Acad. Sci., 117, 18 984–18 990, https://doi.org/10.1073/pnas.2006853117, 2020.
- Wagner, T. and Platt, U.: Satellite mapping of enhanced BrO concentrations in the troposphere, Nature, 395, 486–490, https://doi.org/10.1038/26723, 1998.
 - Wang, C., Graham, R. M., Wang, K., Gerland, S., and Granskog, M. A.: Comparison of ERA5 and ERA-Interim near-surface air temperature, snowfall and precipitation over Arctic sea ice: effects on sea ice thermodynamics and evolution, Cryosphere, 13, 1661–1679, https://doi.org/10.5194/tc-13-1661-2019, 2019a.

- Wang, S., Kinnison, D., Montzka, S. A., Apel, E. C., Hornbrook, R. S., Hills, A. J., Blake, D. R., Barletta, B., Meinardi, S., Sweeney, C., Moore, F., Long, M., Saiz-Lopez, A., Fernandez, R. P., Tilmes, S., Emmons, L. K., and Lamarque, J.-F.: Ocean Biogeochemistry Control on the Marine Emissions of Brominated Very Short-Lived Ozone-Depleting Substances: A Machine-Learning Approach, J. Geophys. Res. Atmos., 124, 12319–12339, https://doi.org/10.1029/2019JD031288, 2019b.
- Wang, S., Mcnamara, S. M., Moore, C. W., Obrist, D., Steffen, A., Shepson, P. B., Staebler, R. M., Raso, A. R. W., Pratt, K. A., and
 Performed, K. A. P.: Direct detection of atmospheric atomic bromine leading to mercury and ozone depletion, ATMOSPHERIC, AND
 PLANETARY SCIENCES, 116, https://doi.org/10.18739/A2D79598P, 2019c.
 - Warwick, N. J., Pyle, J. A., Carver, G. D., Yang, X., Savage, N. H., O'Connor, F. M., and Cox, R. A.: Global modeling of biogenic bromocarbons, J. Geophys. Res.-Atmos., 111, https://doi.org/10.1029/2006JD007264, 2006.
- Weber, J., Shin, Y. M., Staunton Sykes, J., Archer-Nicholls, S., Abraham, N. L., and Archibald, A. T.: Minimal Climate Impacts

 From Short-Lived Climate Forcers Following Emission Reductions Related to the COVID-19 Pandemic, Geophys. Res. Lett., 47, 11,

 https://doi.org/10.1029/2020GL090326, 2020.
 - Wesely, M. L.: Parameterization Of Surface Resistances To Gaseous Dry Deposition In Regional-Scale Numerical-Models, Atmos. Environ., 23, 1293–1304, https://doi.org/10.1016/0004-6981(89)90153-4, 1989.
- Whaley, C. H., Law, K. S., Hjorth, J. L., Skov, H., Arnold, S. R., Langner, J., Pernov, J. B., Bergeron, G., Bourgeois, I., Christensen, J. H.,
 Chien, R.-Y., Deushi, M., Dong, X., Effertz, P., Faluvegi, G., Flanner, M., Fu, J. S., Gauss, M., Huey, G., Im, U., Kivi, R., Marelle, L.,
 Onishi, T., Oshima, N., Petropavlovskikh, I., Peischl, J., Plummer, D. A., Pozzoli, L., Raut, J.-C., Ryerson, T., Skeie, R., Solberg, S.,
 Thomas, M. A., Thompson, C., Tsigaridis, K., Tsyro, S., Turnock, S. T., von Salzen, K., and Tarasick, D. W.: Arctic tropospheric ozone:
 assessment of current knowledge and model performance, Atmos. Chem. Phys., 23, 637–661, https://doi.org/10.5194/acp-23-637-2023,
 2023.
- Wren, S. N., Kahan, T. F., Jumaa, K. B., and Donaldson, D. J.: Spectroscopic studies of the heterogeneous reaction between O3(g) and halides at the surface of frozen salt solutions, J. Geophys. Res. Atmos., 115, 1–8, https://doi.org/10.1029/2010JD013929, 2010.
 - Yang, X., Cox, R. A., Warwick, N. J., Pyle, J. A., Carver, G. D., O'Connor, F. M., and Savage, N. H.: Tropospheric bromine chemistry and its impacts on ozone: A model study, J. Geophys. Res. Atmos., 110, 1–18, https://doi.org/10.1029/2005JD006244, 2005.
- Yang, X., Pyle, J. A., and Cox, R. A.: Sea salt aerosol production and bromine release: Role of snow on sea ice, Geophys. Res. Lett., 35, 1–5, https://doi.org/10.1029/2008GL034536, 2008.
 - Yang, X., Pyle, J. A., Cox, R. A., Theys, N., and Van Roozendael, M.: Snow-sourced bromine and its implications for polar tropospheric ozone, Atmos. Chem. Phys., 10, 7763–7773, https://doi.org/10.5194/acp-10-7763-2010, 2010.
 - Yumashev, D., van Hussen, K., Gille, J., and Whiteman, G.: Towards a balanced view of Arctic shipping: estimating economic impacts of emissions from increased traffic on the Northern Sea Route, Climatic Change, 143, 143–155, https://doi.org/10.1007/s10584-017-1980-6, 2017.

- Zhai, S., Swanson, W., McConnell, J. R., Chellman, N., Opel, T., Sigl, M., Meyer, H., Wang, X., Jaeglé, L., Stutz, J., Dibb, J. E., Fujita, K., and Alexander, B.: Implications of Snowpack Reactive Bromine Production for Arctic Ice Core Bromine Preservation, J. Geophys. Res. Atmos., 128, e2023JD039 257, https://doi.org/10.1029/2023JD039257, 2023.
- Zhao, X., Strong, K., Adams, C., Schofield, R., Yang, X., Richter, A., Friess, U., Blechschmidt, A.-M., and Koo, J.-H.: A case study of a transported bromine explosion event in the Canadian high arctic, J. Geophys. Res. Atmos., 121, 457–477, https://doi.org/10.1002/2015JD023711, 2016.